CHAPTER 5

Results and Discussion (Part II):

Powders and Ceramics in the (1-x)PMN-xPT System

In this section, the comprehensive studies on optimizing the key parameters, thereby demonstrating the validity of the mixed oxide technique for the PMN-PT system, are bought out and discussed.

5.1 Powders in the (1-x)PMN- xPT system

Compositions in the pseudo-binary system (1-x)PMN-xPT ($0.1 \leq x \leq 0.9$; $\Delta x = 0.1$) have been prepared from PMN and PT precursor powders, employing a combination of a simple mixed oxide synthetic route and a rapid vibro-milling technique. Attention was focused on relationships between composition, phase formation and morphology. Concentrations of perovskite phase, optimum calcination conditions and grain size of the entire compositional range are given in Table 5.1.

Table 5.1 Phase formation and grain size of powders in the (1-x)PMN-xPT system at their optimum conditions.

Composition (x)	Optimum calcination condition (°C for 2 h) with heating/cooling rates of 20 °C/min	Concentration of perovskite phase (%)	Grain size* (μm)
0.1	900	100	0.18-0.52
0.2	850	100	0.16-0.65
0.3	800	100	0.25-0.54
0.4	800	100	0.26-0.60
0.5	750	100	0.22-0.58
0.6	750	100	0.18-0.62
0.7	700	100	0.24-0.61
0.8	650	100	0.27-0.55
0.9	600	100	0.36-0.62

* These data were taken by estimating from SEM-micrographs

5.1.1 Phase analysis

The X-ray diffraction patterns from calcined powders with maximum perovskite phase are given in Fig. 5.1, for all compositions, which support the existence of perovskite solid solutions as the sole phase present. No significant amounts of pyrochlore phase were detected within the limitations of XRD method. This observation indicates that the use of high purity PMN and PT precursors at optimum firing temperatures can effectively enhance the yield of the perovskite phase.

In general, similar XRD patterns, indicating the formation of a single perovskite solid solution phase, were observed in all compositions. Optimum calcination conditions for all powders were established by identifying the conditions for maximising the yield of perovskite. It is evident that the optimum calcination temperature decreases with increasing PT content (Table 5.1), in agreement with earlier work on PT-based materials.[128]

A gradual shift of diffraction peaks towards higher-2θ angles is observed with increasing the PT content. Meanwhile, distinct increases in peaks splitting (e.g. those of (001)-(100), (101)-(110), (002)-(200) and (112)-(211) reflections) with increasing values of x are noticeable (Fig. 5.2 (a)-(d)), which is undoubtedly attributed to the gradual phase transition. For example, the XRD spectra of the (200) reflection for the (1-x)PMN-xPT powders (calcined at their optimum temperatures) with various x-values are shown in Fig. 5.3. Lattice parameters of the unit cell were calculated from the XRD data and the results are compared in Fig. 5.4, along with tetragonality factors (or axial ratios of c/a) and average lattice parameters of $(a^2c)^{1/3}$.

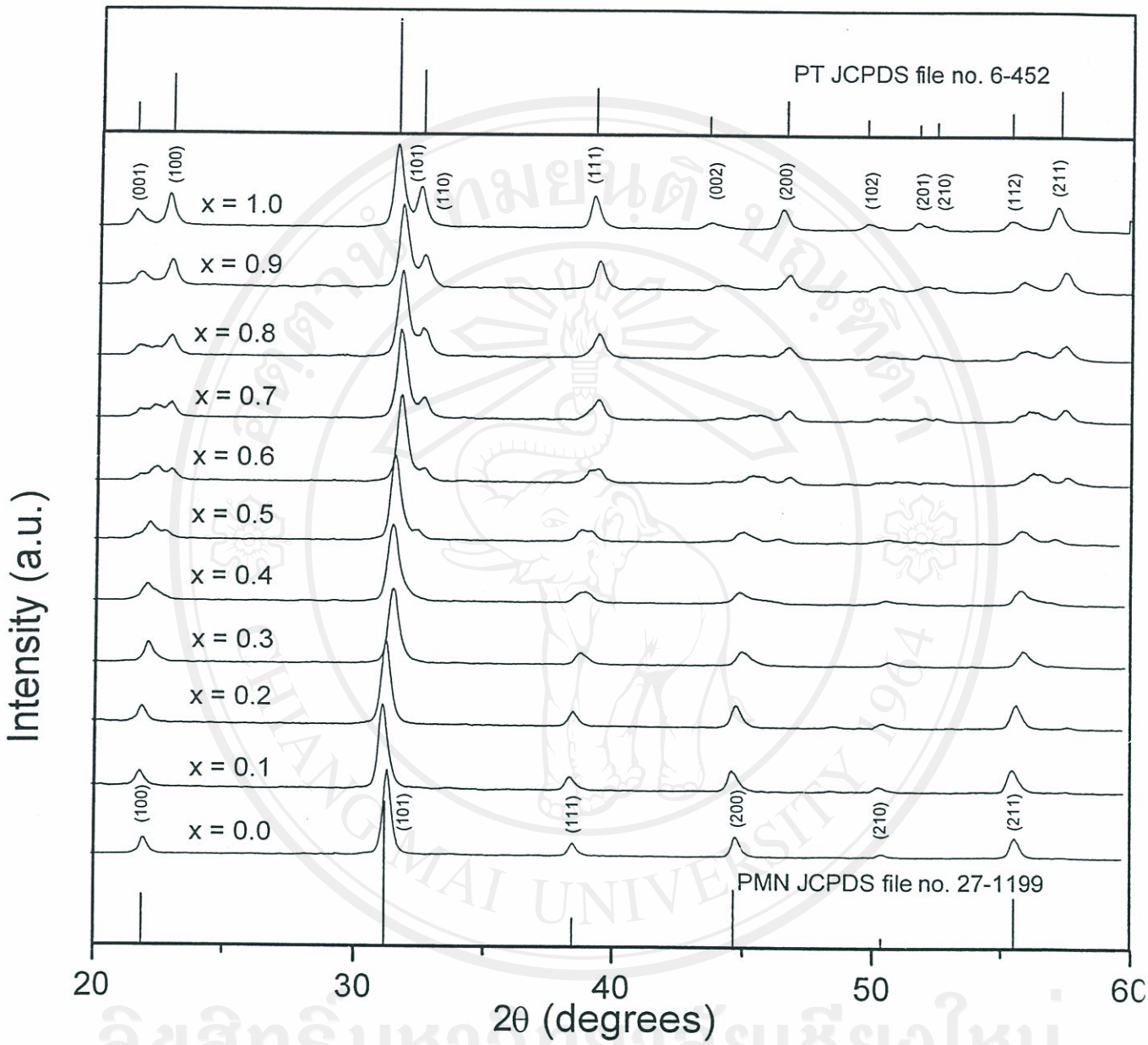

Fig. 5.1 XRD patterns of the (1-*x*)PMN-*x*PT powders calcined at their optimum conditions.

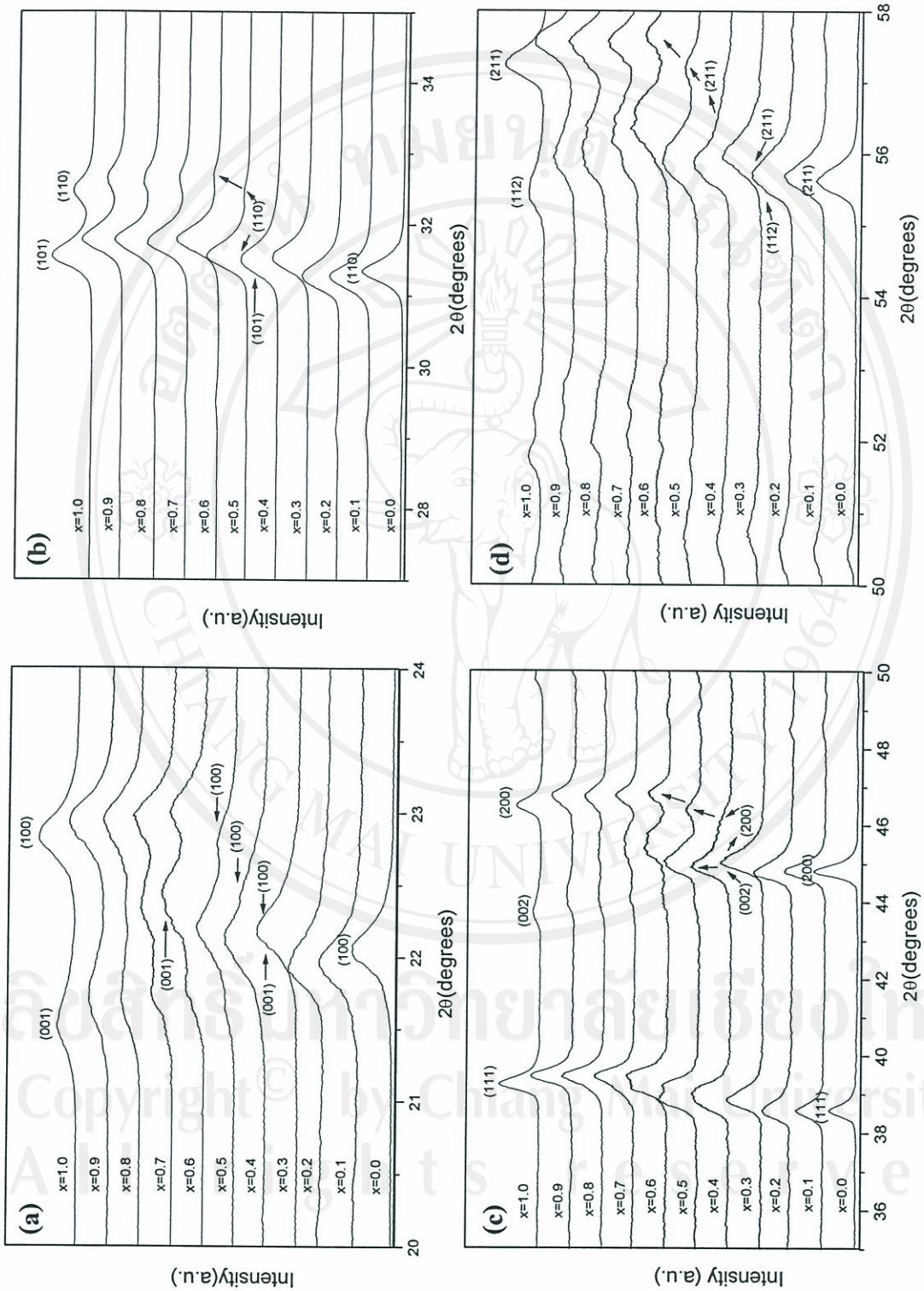

Fig. 5.2 Selected regions of the diffraction patterns for calcined powders in the (1-x)PMN-xPT system.

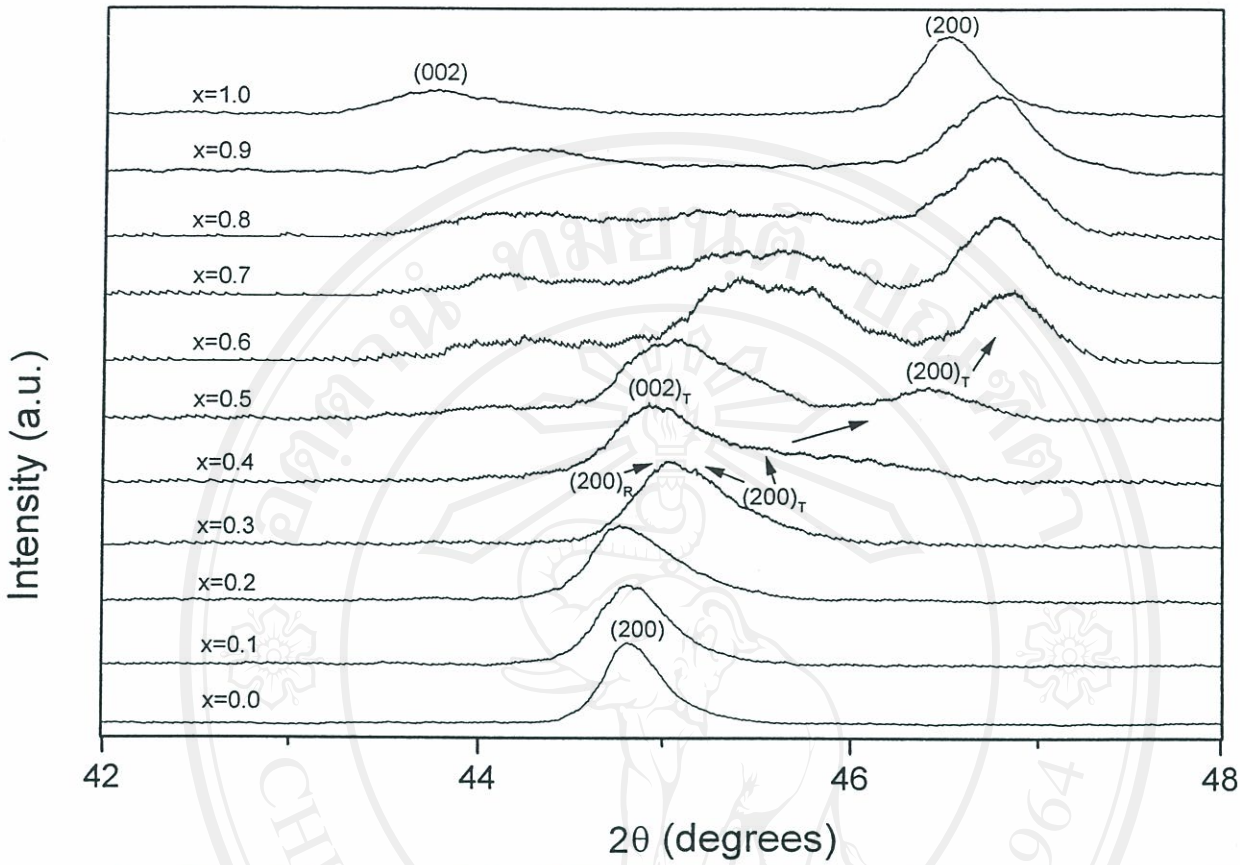

Fig. 5.3 XRD patterns of the (200) reflection for the (1-*x*)PMN-*x*PT powders with different *x* values.

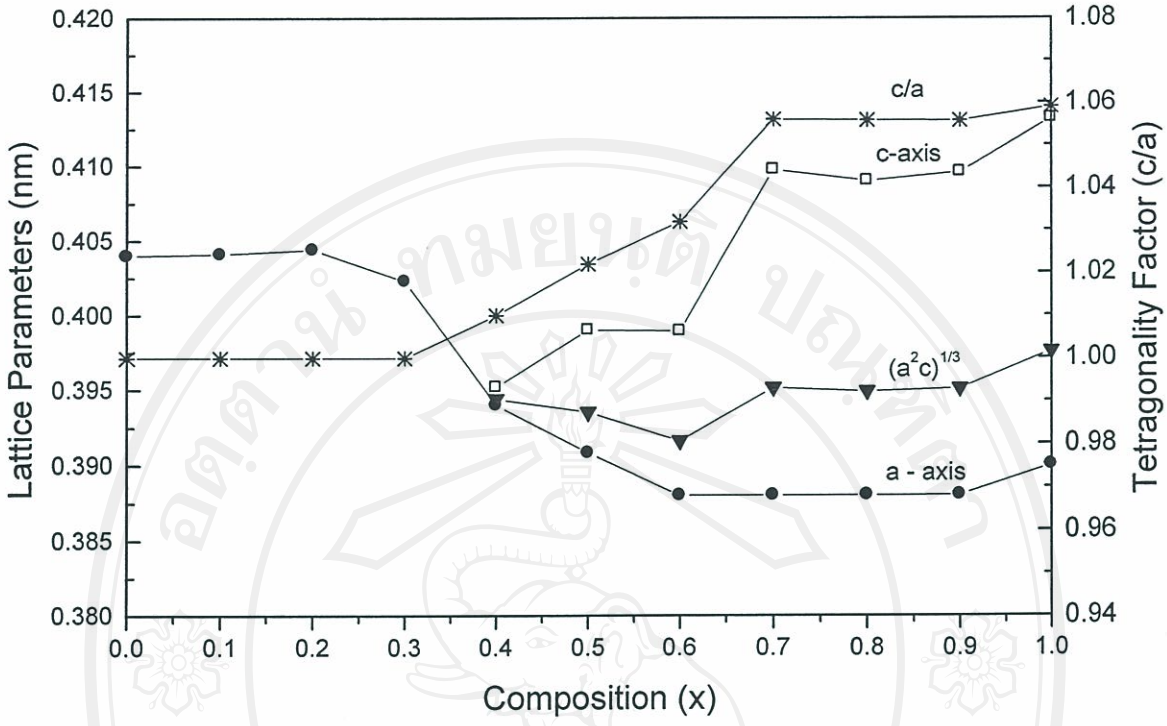

Fig. 5.4 Lattice parameters and tetragonality factor (*c/a*) of the (1-*x*)PMN-*x*PT powders.

The parameters of (pseudo) cubic PMN ($x = 0.0$) and tetragonal PT ($x = 1.0$) are 0.404 nm, and $a = 0.390$ and $c = 0.413$ nm, respectively, which are virtually identical to reported data (JCPDS file no. 27-1199 and 6-452, respectively). Only a (pseudo) cubic symmetry was observed at low values of PT content, in good agreement with other workers.[129,130,131] A single and sharp peak is observed in PMN-PT powders with $0.0 \leq x \leq 0.2$. The broadening of the peak increases as the *x*-value increases from 0.0 to 0.2. Recent work by Fengbing *et al.*[129] and Noheda *et al.*[133] show that the perovskite phases of PMN-PT undergo the transitions (pseudo) cubic $\rightarrow$ rhombohedral at $x \sim 0.2$, due to lattice deformation.

It is interesting to note that when *x*-value changes from 0.2 to 0.3, the (200) reflection splits into two and the intensity of $(200)_T$ increases simultaneously, in consistent with Fengbing *et al.*[129] At $x = 0.4$, however, peak splittings are well defined

in Fig. 5.3, with a = 0.394, c = 0.396 nm, and c/a = 1.01 as shown in Fig. 5.4. This observation indicates that the peaks separate completely from each other, which exhibits the analogous characteristic as common ferroelectrics PT (x = 1.0). From the crystallographic analyses, therefore, the phase boundaries between the rhombohedral and tetragonal symmetries seem to be located at $0.3 < x < 0.4$. This composition range is very close to the morphotropic phase boundary (MPB) of the PMN-PT system reported by a number of workers.[129,130,131,132] The detail of peak splitting within this region have been well-described by Noheda *et al.*[133] where the synchrotron X-ray powder diffraction have been performed. Their results indicate that the MPB of the PMN-PT system contains multiphase components (including orthorhombic and monoclinic phases) and complex phase behaviour. Thus, futher experimental and theoretical work still be required for more systematic studies to be properly understood and to clarify more precisely the nature of the MPB of the PMN-PT system.

With further increases in x-value from 0.4 to 0.6, the a-axis shrunk while the c-axis expanded continuously at approximately similar rates. Consequently, the values of $(a^2c)^{1/3}$ decreased slowly, while the axial ratios of c/a increased rapidly to 1.03. It is interesting to note that lattice parameters (a and c-axis, and $(a^2c)^{1/3}$) and tetragonality factor (c/a) tend to be stable for $0.7 \leq x \leq 0.9$ and then slightly increases as the x-value increases from 0.9 to 1.0. By comparing the B-site cation sizes of PMN and PT (0.0667 vs. 0.0605 nm),[129] the continuous decrease in the average lattice parameter (from 0.404 nm at x = 0.0 to 0.397 nm at x = 1.0) can be well understood, which supports the formation of complete crystalline solutions of a perovskite structure.

5.1.2 Morphological analysis

SEM micrographs of the calcined (1-x)PMN-xPT powders are shown in Figs. 5.5 (a)-(e) and 5.6 (a)-(d), indicating representative morphologies. These samples were calcined at their optimum temperatures. In general, similar morphological

characteristics were observed in these powders, i.e. agglomerated and basically irregular in shape, with a substantial variation in particle size. However, some spherical particles can be found in some micrographs e.g. Figs. 5.5 (b-e) and 5.6 (a). The range of particle diameter was found to be about 100-700 nm. Kong *et al.*[134] have also reported that their attempts to prepare nanometer-sized PMN-PT powders (~ 20-50 nm) via a high-energy ball milling process were successful.

Corresponding EDX analysis and chemical compositions for some of these (1-*x*)PMN-*x*PT powders are shown in Figs. 5.7 (a)-(d) and Table 5.2. It is indicated that the (1-x)PMN-*x*PT powders with different compositions are composed of a variation in Mg/Nb/Ti ratios. It was observed that the Ti concentration increases with increasing PT content. The combination of X-ray and SEM/EDX results strongly support that in this study, the series of (1-*x*)PMN-*x*PT solid solution were formed.

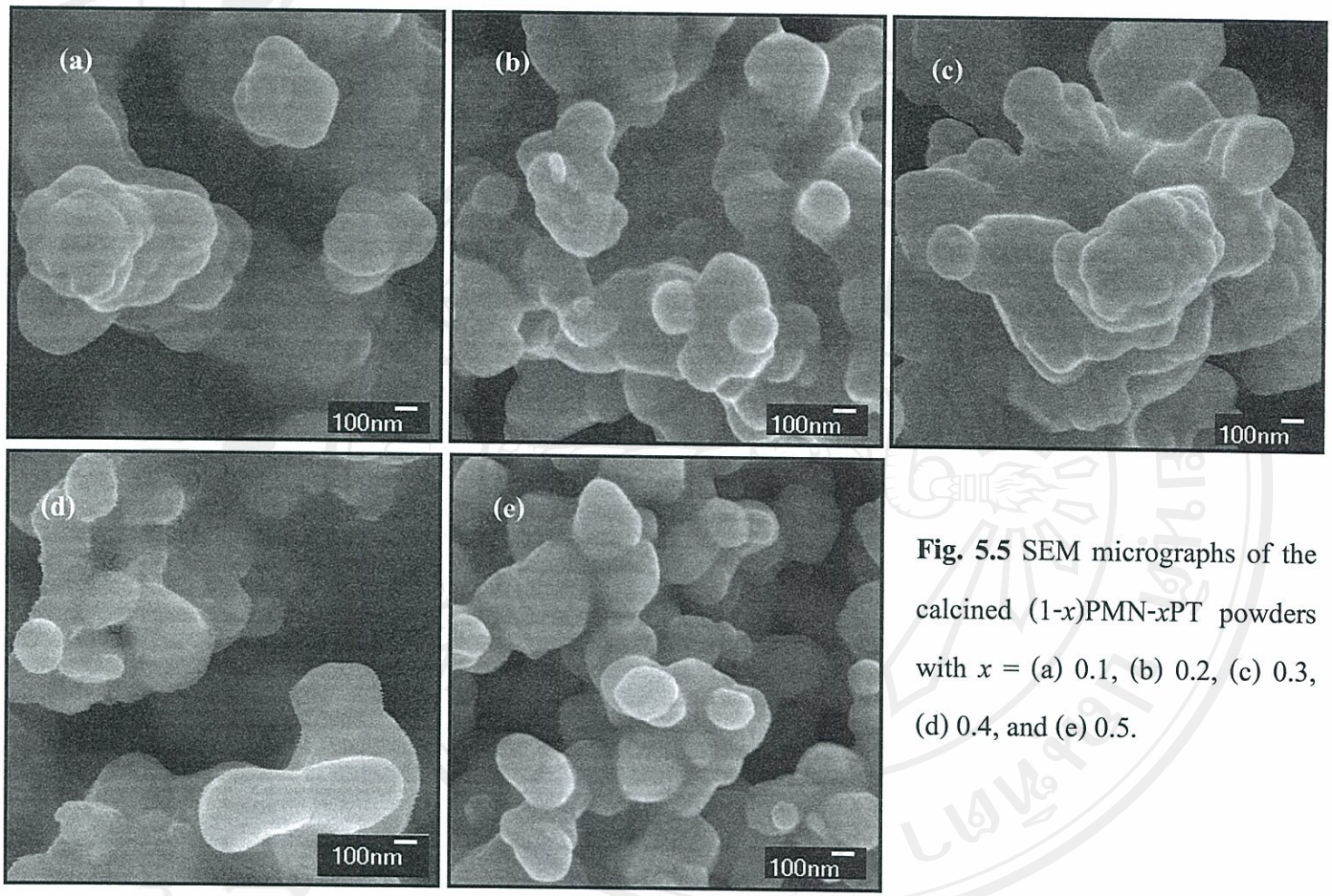

Fig. 5.5 SEM micrographs of the calcined (1-x)PMN-xPT powders with x = (a) 0.1, (b) 0.2, (c) 0.3, (d) 0.4, and (e) 0.5.

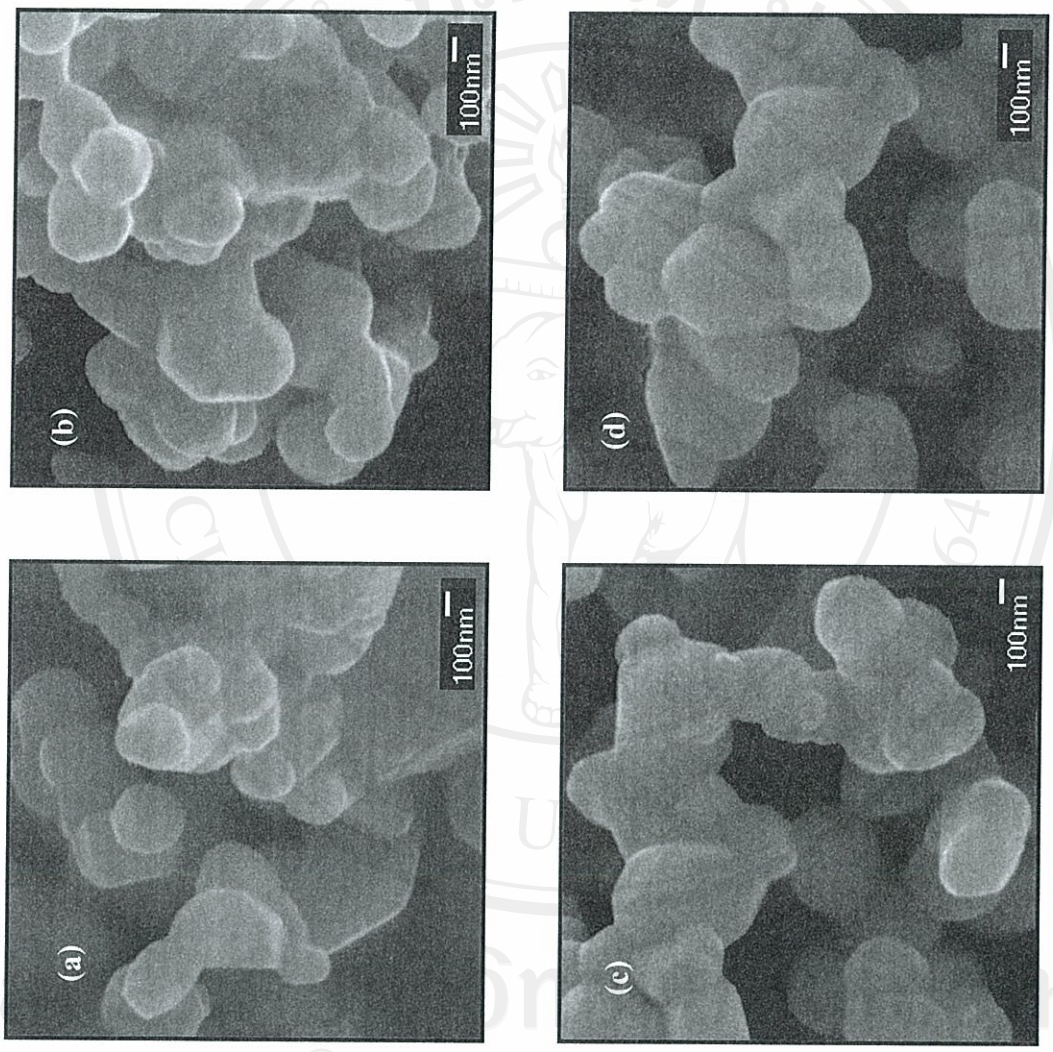

Fig. 5.6 SEM micrographs of the calcined (1-x)PMN-xPT powders with x = (a) 0.6, (b) 0.7, (c) 0.8, and (d) 0.9.

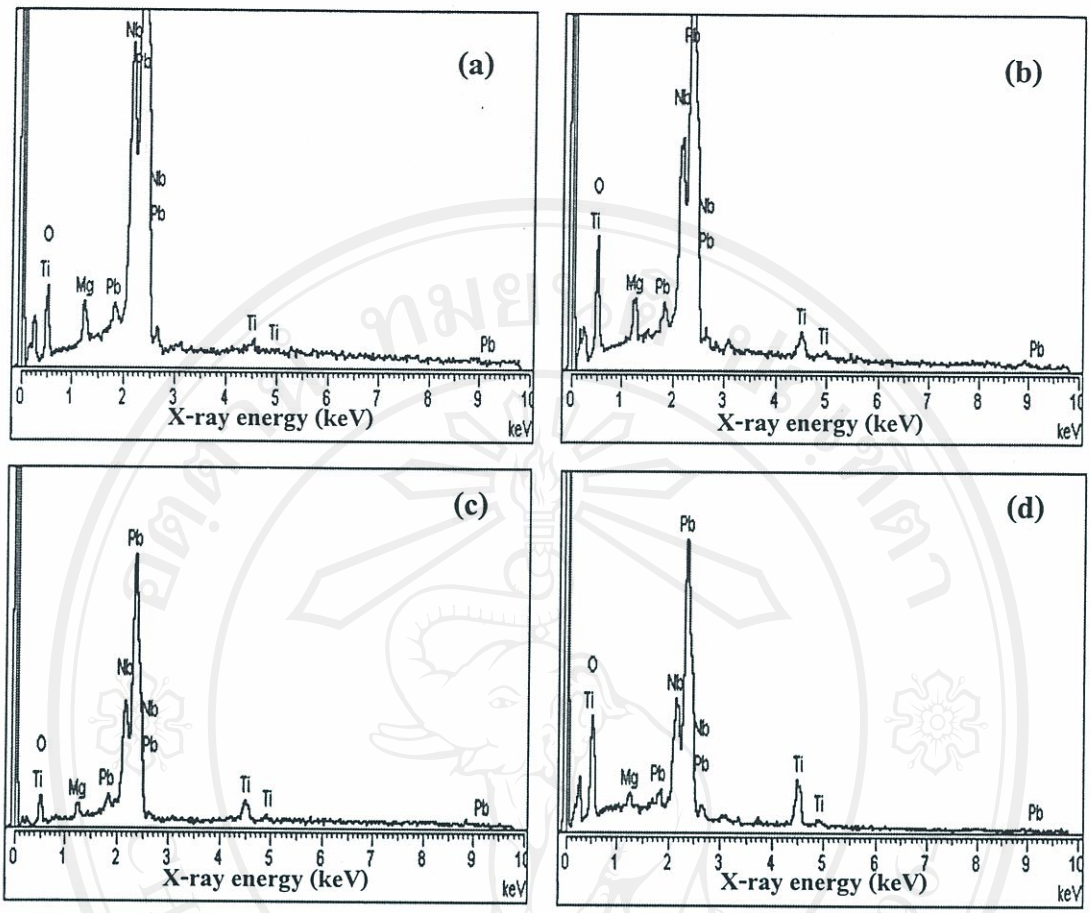

Fig. 5.7 EDX analysis of the calcined (1-x)PMN-xPT powders with x = (a) 0.1, (b) 0.2, (c) 0.3, and (d) 0.4.

Table 5.2 Chemical compositions of the calcined (1-x)PMN-xPT powders from EDX analysis.

Compositions (at%)				Possible phases
Pb(M)	Ti(K)	Mg(K)	Nb(L)	
11.90	7.93	1.74	7.61	0.6PMN-0.4PT
12.61	3.32	3.79	11.88	0.7PMN-0.3PT
15.11	3.18	4.32	12.06	0.8PMN-0.2PT
20.76	1.43	4.74	19.62	0.9PMN-0.1PT

5.2 Powders in the 0.9PMN-0.1PT system

In order to investigate the effect of processing conditions on phase formation and morphology of the compound in the (1-*x*)PMN-*x*PT system further, powder of 0.9PMN-0.1PT was chosen as described here.

5.2.1 Thermal analysis

The TG and DTA curves recorded at a heating rate of 10 °C/min in air for an equimolar mixture of $MgNb_2O_6$, PbO and TiO_2 by weighting of 0.9PMN-0.1PT is shown in Fig. 5.8. It is seen that TG curve demonstrates two distinct weight loss below 400 °C. The first weight loss occurs below 200 °C and the second one above 250 °C. In the temperature range from room temperature to ~ 150 °C, the sample shows small exothermic peak in the DTA curve at 120 °C, which are related to the first weight loss. This DTA peak can be attribute to the decomposition of organic species from milling process.[42] After the first weight loss, the sample shows a sharp fall in specimen weight with increasing temperature from 240-300 °C.

Corresponding to the second fall in specimen weight (~ 1.4 %), by increasing the temperature up to ~ 750 °C, the solid-state reaction occurs between PbO, TiO_2 and $MgNb_2O_6$. The broad exothermic characteristic in the DTA curve represents that reaction, which has a maximum at ~ 500 °C. Moreover, another exothermic peaks with maximum at 600 °C and 700 °C were also observed in this profile. These temperatures have been obtained from the calibration of the sample thermocouple.

These data were used to define the ranges of temperatures (500 to 900 °C) for XRD investigation. All calcined powders, together with that of the starting powder mixtures were examined by XRD in order to investigate the phase development (Figs. 5.2-5.4).

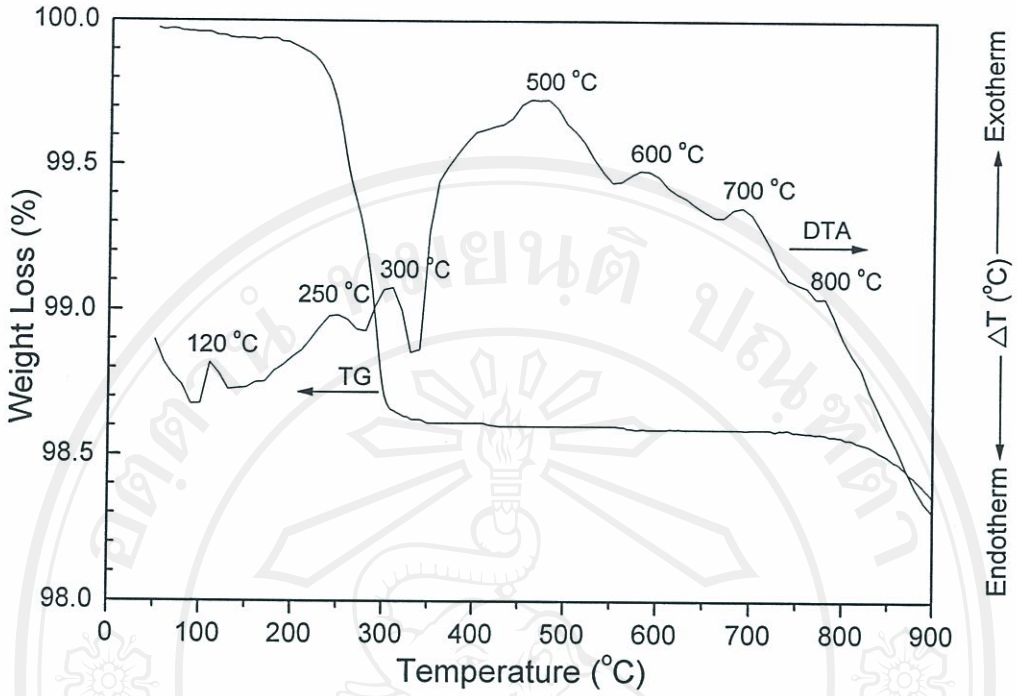

Fig. 5.8 TG and DTA curves for the mixture of PbO-TiO_2-$MgNb_2O_6$ powders.

5.2.2 Phase analysis

The effect of calcination conditions on phase formation behaviour of 0.9PMN-0.1PT was also examined. X-ray diffraction patterns of 0.9PMN-0.1PT powders calcined at various conditions are given in Figs. 5.9-5.11, indicating the formation of both perovskite and pyrochlore phases. Figure 5.9 was shown the phase formation of 0.9PMN-0.1PT powders with calcinations temperature conditions. The formation of pyrochlore phase ($Pb_3Nb_4O_{13}$) has been initially found at 600 °C. The strongest reflections in the majority of the XRD patterns indicate the formation of perovskite phase of lead magnesium niobate-lead titanate, 0.9PMN-0.1PT powders. In this study, a single phase of perovskite 0.9PMN-0.1PT was found in the samples calcined at temperature 900 °C.

Having established the optimum calcination temperature, alternative dwell times ranging from 0.5 to 3 h with constant heating/cooling rates of 20 °C/min were

applied at 900 °C, as shown in Fig. 5.10. It is seen that the single phase of perovskite 0.9PMN-0.1PT (yield of 100% within the limitations of the XRD technique) was found to be possible only in powder, calcined at 900 °C for at least of 2 h or more. The appearance of $Pb_3Nb_4O_{13}$ phases in some XRD patterns indicated that full crystallization have not occurred at relatively shorter calcination times. The observation that the dwell times effect may also play an important role in obtaining a single-phase perovskite product is also consistent with other similar systems.[15,16]

Apart from the calcination temperature and dwell time, the effect of heating/cooling rates on the formation behaviour of PMN-PT was also investigated. Six heating/cooling rates (3, 5, 10, 15, 20 and 30 °C/min) were selected for calcination condition of 900 °C/2h (Fig. 5.11). In this connection, it is shown that the yield of 0.9PMN-0.1PT phase did not vary significantly with heating/cooling rates, indicating that fast heating/cooling rates can leads to full crystallization of 0.9PMN-0.1PT phase without time for the formation of pyrochlore phase or lead vaporization. The observation that faster heating/cooling rates are required for lead-based ferroelectrics is also consistent with other investigators.[135,136]

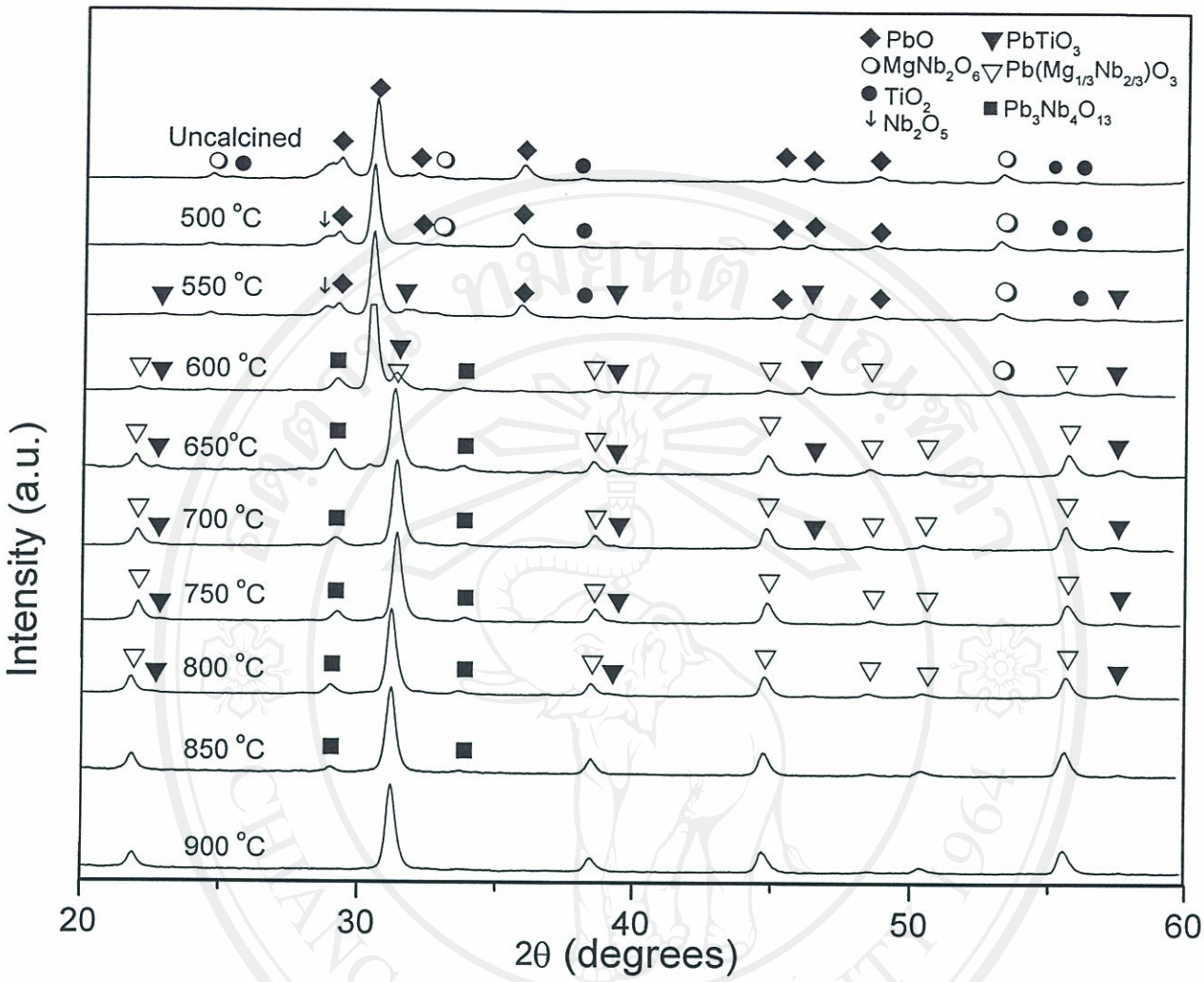

Fig. 5.9 XRD patterns of 0.9PMN-0.1PT powders calcined at various temperatures for 2 h with heating/cooling rates of 20 °C/min.

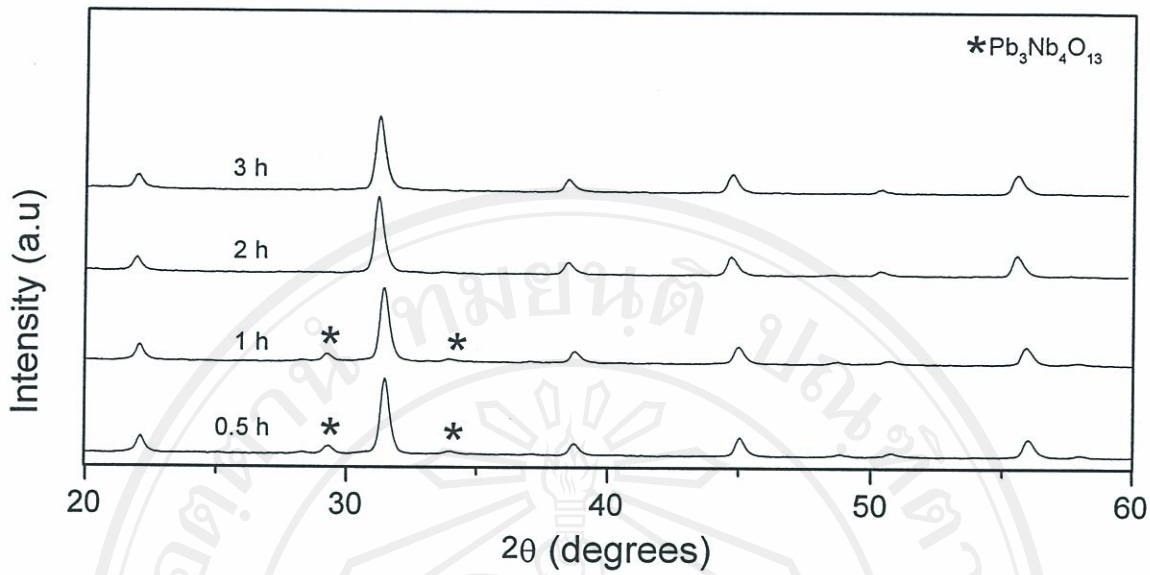

Fig. 5.10 XRD patterns of 0.9PMN-0.1PT powders calcined at 900 °C with heating/cooling rates of 20 °C/min for various dwell times.

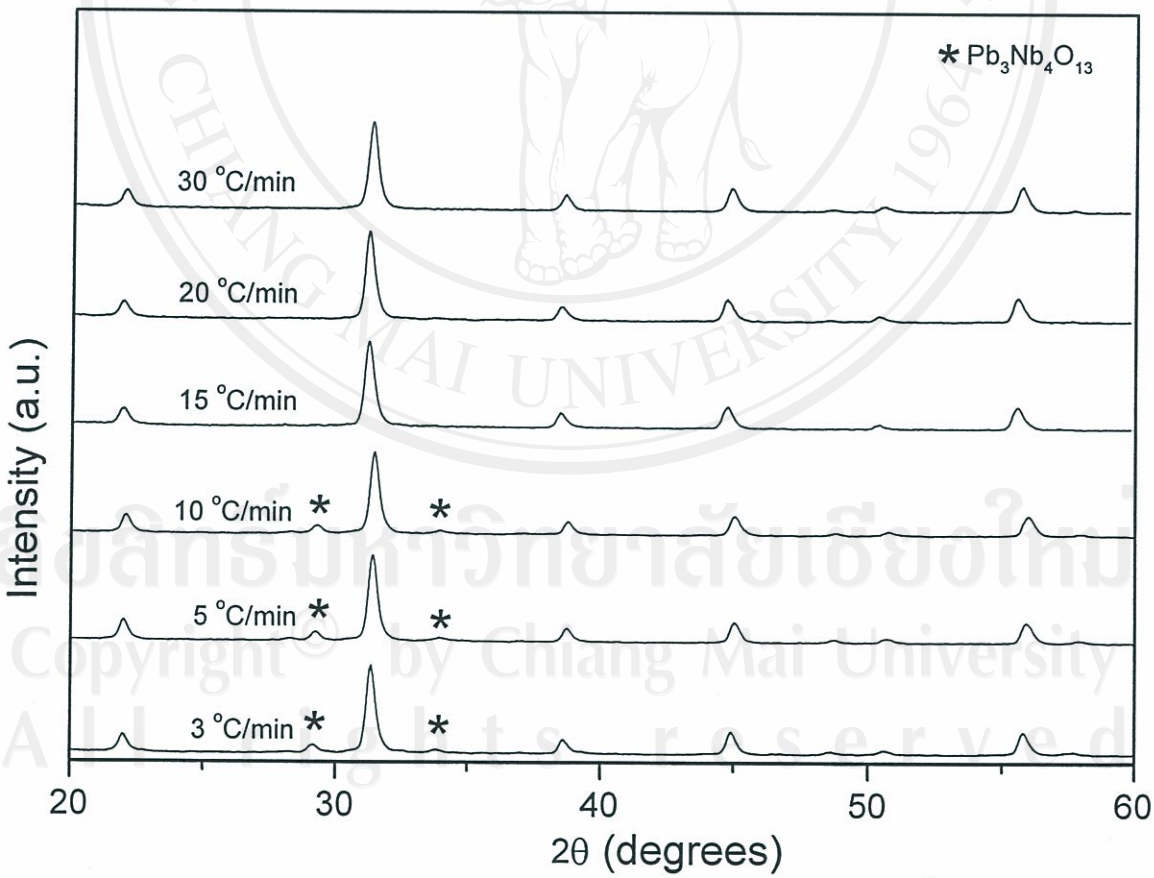

Fig. 5.11 XRD patterns of 0.9PMN-0.1PT powders calcined at 900 °C for 2 h with various heating/cooling rates.

5.2.3 Morphological analysis

The morphological evolution during calcination was investigated by scanning electron microscopy (SEM). Micrographs of the 0.9PMN-0.1PT powders calcined at 850 °C for 2 h and 900 °C for 2 and 3 h with various heating/cooling rates of 20 °C/min and calcined at 900 °C for 2 h with various heating/cooling rates from 5 to 30 °C/min are shown in Figs. 5.12 (a-f). The range of particle diameter was found to be about 100-500 nm. In general, the particles are agglomerated and basically irregular coexist with spherical in shape, with a substantial variation in particle size, particularly in samples calcined for longer dwell time or with faster heating/cooling rates.

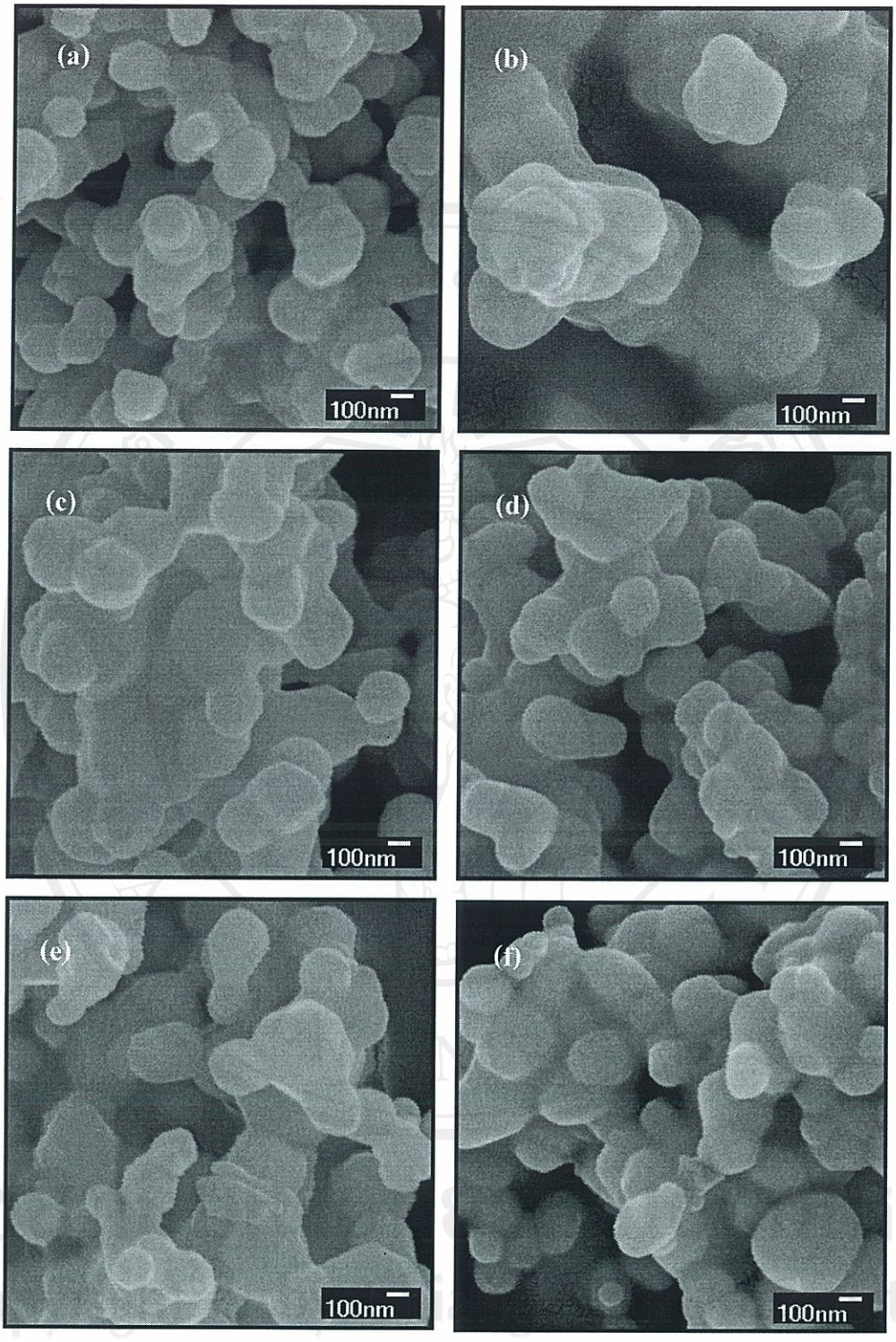

Fig. 5.12 SEM micrographs of the 0.9PMN-0.1PT powders calcined at (a) 850 °C/2 h , (b) 900 °C/2 h, and (c) 900 °C/3 h with heating/cooling rates of 20 °C/min and calcined at 900 °C/2 h with heating/cooling rates of (d) 5 °C/min, (e) 15 °C/min and (f) 30 °C/min.

5.3 Ceramics in the (1-x)PMN-xPT system

Since the PMN-PT compositions having high PT content in the range $0.6 \leq x \leq 0.9$; $\Delta x = 0.1$) could not be fabricated as a bulk form of high density, these compositions could not be characterized any further for the rest of the study. Their comparatively large c/a values, which give rise to serious internal stress, are responsible for the frequent crack developments around the phase transition temperature during cooling of these sintered samples. In the present study, only compositions in the pseudo-binary system (1-x)PMN-xPT ($0.1 \leq x \leq 0.5$; $\Delta x = 0.1$) have been successfully fabricated from the calcined (1-x)PMN-xPT powders, employing a normal sintering method, i.e. pressurless sintering technique.

Attention was focused on relationships between sintering conditions, phase formation, densification and microstructure. Calculated relative densities, shrinkage, weight loss, concentrations of perovskite phase and optimum sintering conditions of the entire compositional range are given in Table 5.3.

Table 5.3 Phase formation and densification characteristics of ceramics in the (1-x)PMN-xPT system at their optimum conditions.

Composition (x)	Optimum sintering conditions (^{o}C for 2 h)	Concentration of perovskite phase (%)	Density* (g/cm^3)	Shrinkage (%)	Weight loss (%)
0.1	1240	100	7.98	14.92	12.75
0.2	1240	100	7.94	15.29	12.54
0.3	1240	100	7.86	13.17	12.23
0.4	1220	100	7.83	12.32	12.37
0.5	1220	100	7.78	12.40	12.46

* Theoretical density values of the (1-x)PMN-xPT system are not available in the ICDD data based at the present time.

5.3.1 Phase analysis

The X-ray diffraction patterns from sintered ceramics with maximum perovskite phase and bulk density are presented in Fig. 5.13, where complete crystalline solutions of perovskite structure were formed throughout the whole composition ranges. Optimum sintering conditions for all ceramics were established by identifying the conditions for maximizing both the bulk density and the yield of perovskite. It is evident that similar optimum sintering conditions of 1240 ^{o}C for 2 h with 15 ^{o}C/min, were observed in samples at compositions of x between 0.1 to 0.3 whilst for compositions with PT content of x = 0.4 and 0.5 optimum condition was found at 1220 ^{o}C for 2 h with 15 ^{o}C/min, although the optimum sintering temperature of PMN is slightly higher than that of PT (see Sections 4.1.3 and 4.2.2).

In general, only a (pseudo) cubic symmetry was observed at low values of PT concentration, in good agreement with other workers.[134,137] By the influence of PT, however, several peaks split for $x \geq 0.4$, indicating the development of tetragonal symmetry, which continued with a further increase in PT concentration. For example, (002)-(200) peaks splitting the diffraction line around 2θ of 44-46 ° are shown in Fig. 5.14, confirming their tetragonal symmetry, in consistent with earlier work on PMN-PT ceramics.[91,92] By considering the degrees of peak splitting at $x = 0.4$, the onset composition for the tetragonal symmetry development seems to be just below $x = 0.4$.

The effect of PT content on the lattice parameters of the composition in the PMN-PT ceramics are given in Fig. 5.15. Crystal symmetries of the perovskite solid solutions were (pseudo) cubic at $x = 0.0$ to 0.2, while tetragonal symmetries started to develop at $x = 0.3$, with the degrees of peak splitting increasing at higher PT concentrations. As the precise onset compositions of the tetragonal symmetry development (although somewhat below $x = 0.4$, as discussed in Fig. 5.14) are not clear in Fig. 5.15, more work needs to be conducted in the range of $0.2 < x < 0.4$ for close determination of the compositions. With further increase in the PT concentration, values of the lattice parameter c increased, while those of a decreased, thus resulting in rapid increases in the tetragonality factor (or the axial ratio) of c/a to 1.02.

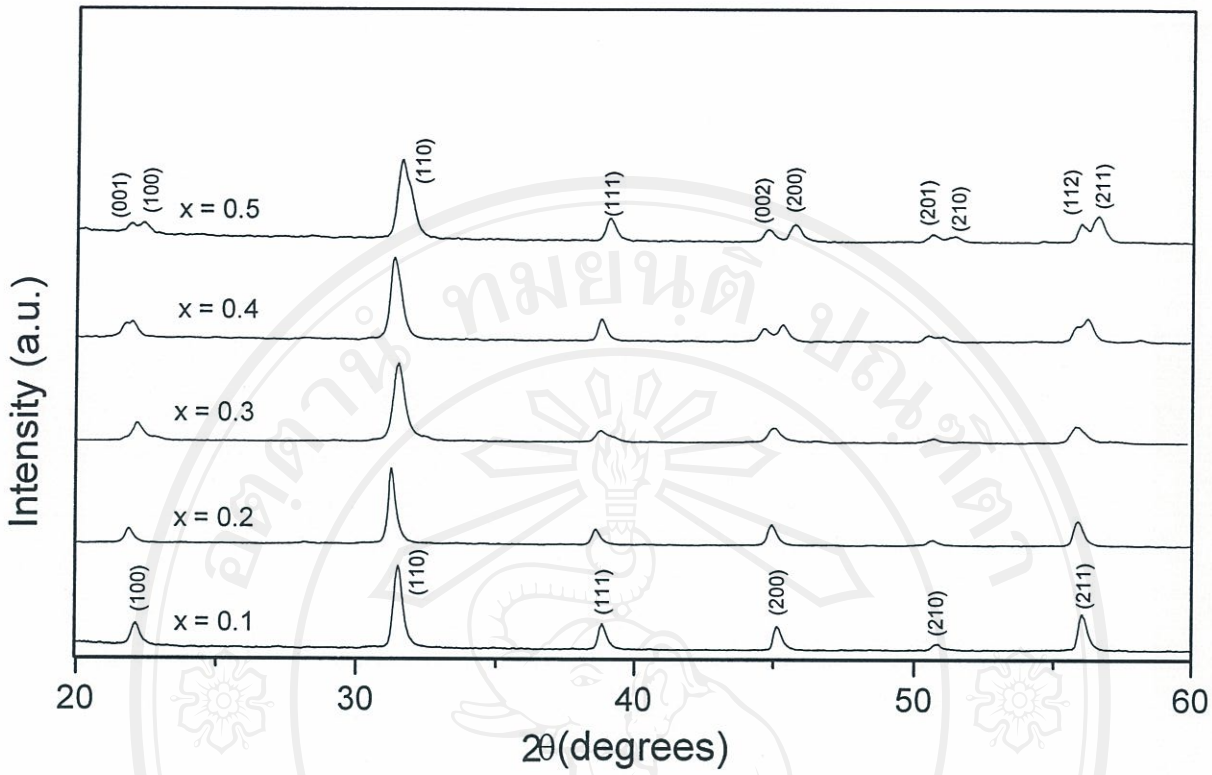

Fig. 5.13 XRD patterns of the (1-*x*)PMN-*x*PT ceramics sintered at their optimum conditions.

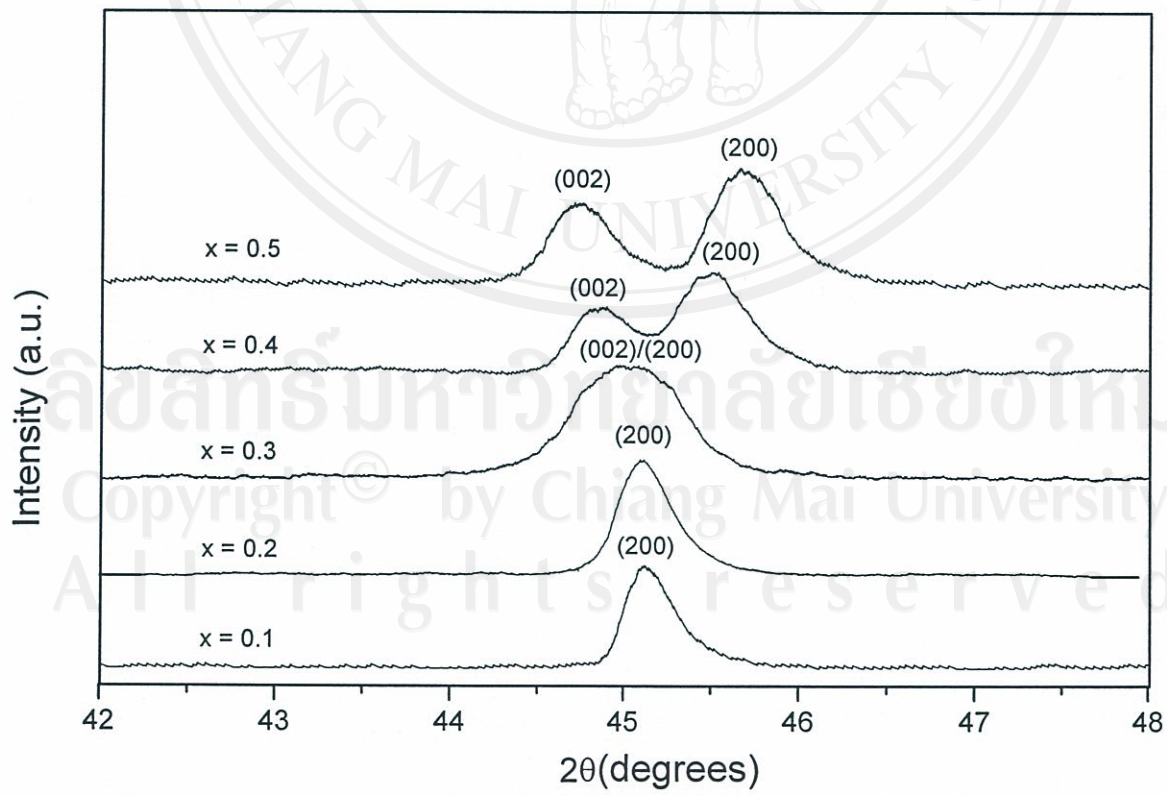

Fig. 5.14 XRD patterns of (002)-(200) reflections for the (1-*x*)PMN-*x*PT ceramics with different *x*-values.

For comparison, the parameter of PMN is 0.4045 to 0.4046 nm,[138] which is the one at x = 0.0. The steady decreases in the average lattice parameter $(a^2c)^{1/3}$ with increasing PT concentration can be well explained by the cation replacements of smaller Ti (0.0605 nm) for Nb (0.064 nm) and much larger Mg (0.0720 nm), which would lead to gradural contraction in the unit cell dimensions, and finally resulting in fragility.[139]

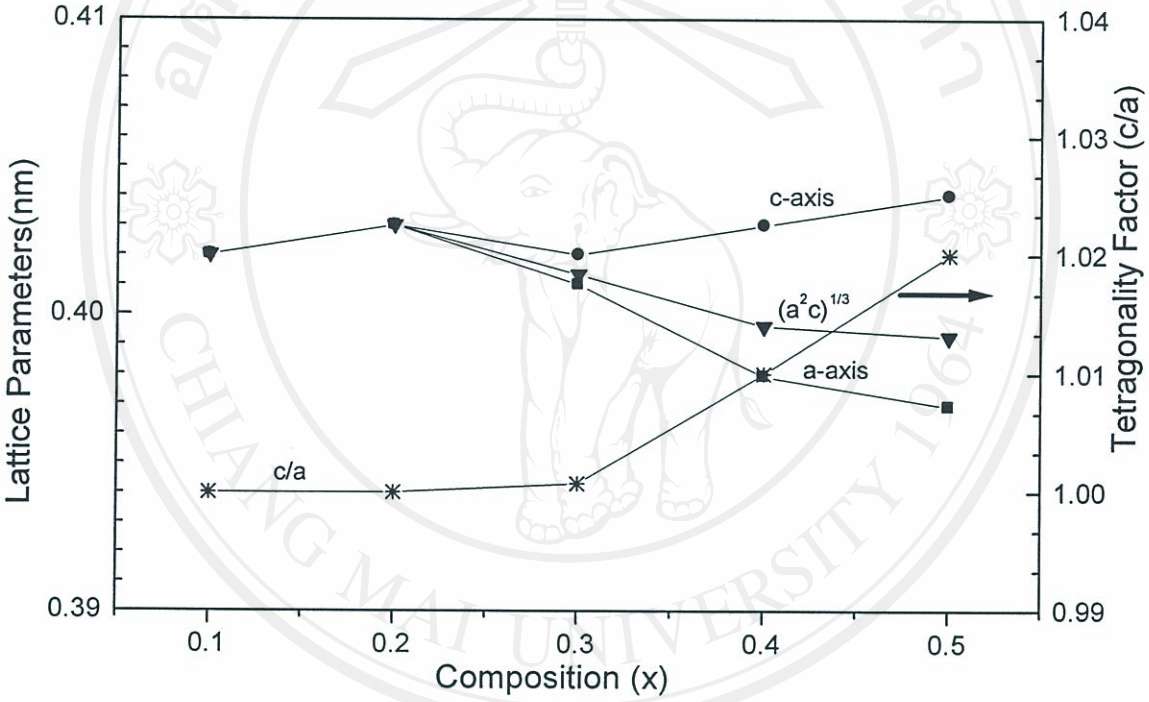

Fig. 5.15 Variation of cell parameters and tetragonality factor in the (1-x)PMN-xPT system.

The effect of sintering conditions on phase formation behavior of other compositions e.g. 0.5PMN-0.5PT, 0.6PMN-0.4PT, 0.7PMN-0.3PT, 0.8PMN-0.2PT and 0.9PMN-0.1PT, and was also investigated as shown in Figs. 5.16 to 5.20. Similar results were found in all these compositions except for 0.5PMN-0.5PT where perovskite phase is the only detectable phase after sintering between 1180 and

1270 °C, as shown in Fig. 5.16. In order to evaluate the concentration of perovskite and pyrochlore phase, equation (3.4) was applied to these XRD patterns with results given in Tables 5.4 to 5.8.

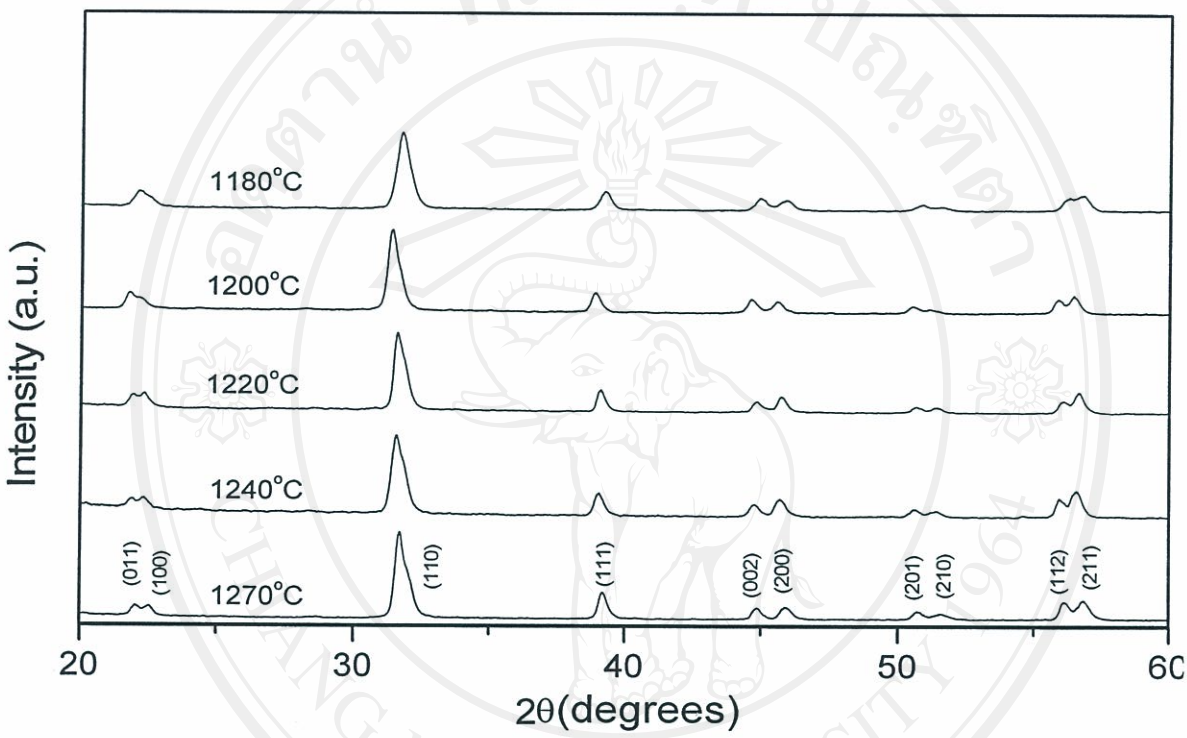

Fig. 5.16 XRD patterns of 0.5PMN-0.5PT ceramics sintered at various temperatures for 2 h with heating/cooling rates at 15 °C/min.

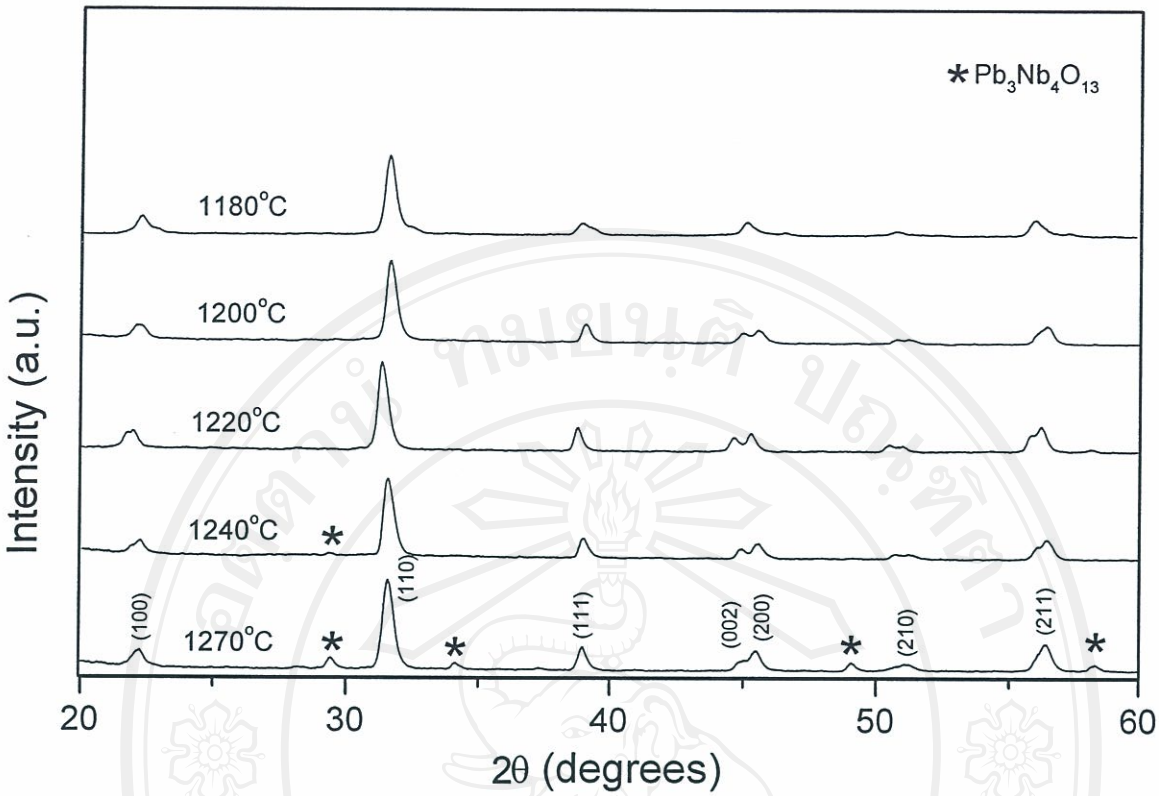

Fig. 5.17 XRD patterns of 0.6PMN-0.4PT ceramics sintered at various temperatures for 2 h with heating/cooling rates at 15 °C/min.

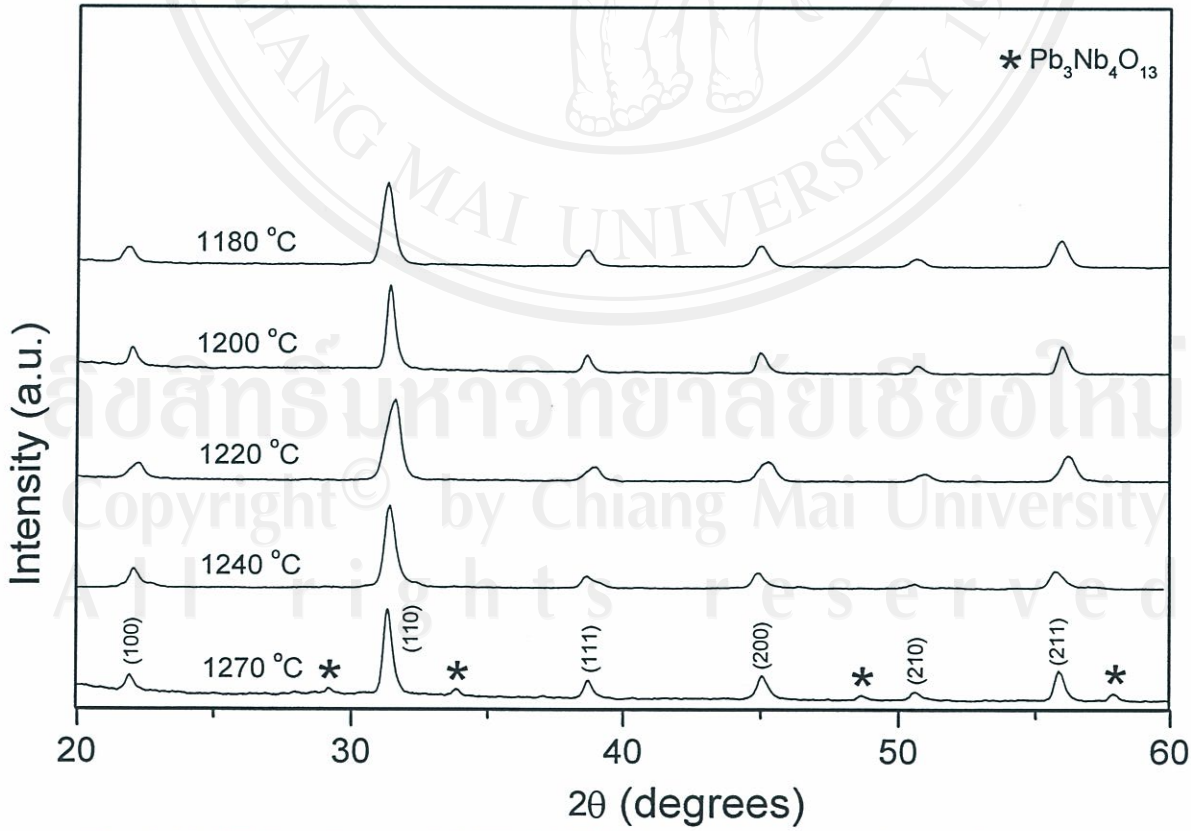

Fig. 5.18 XRD patterns of 0.7PMN-0.3PT ceramics sintered at various temperatures for 2 h with heating/cooling rates at 15 °C/min.

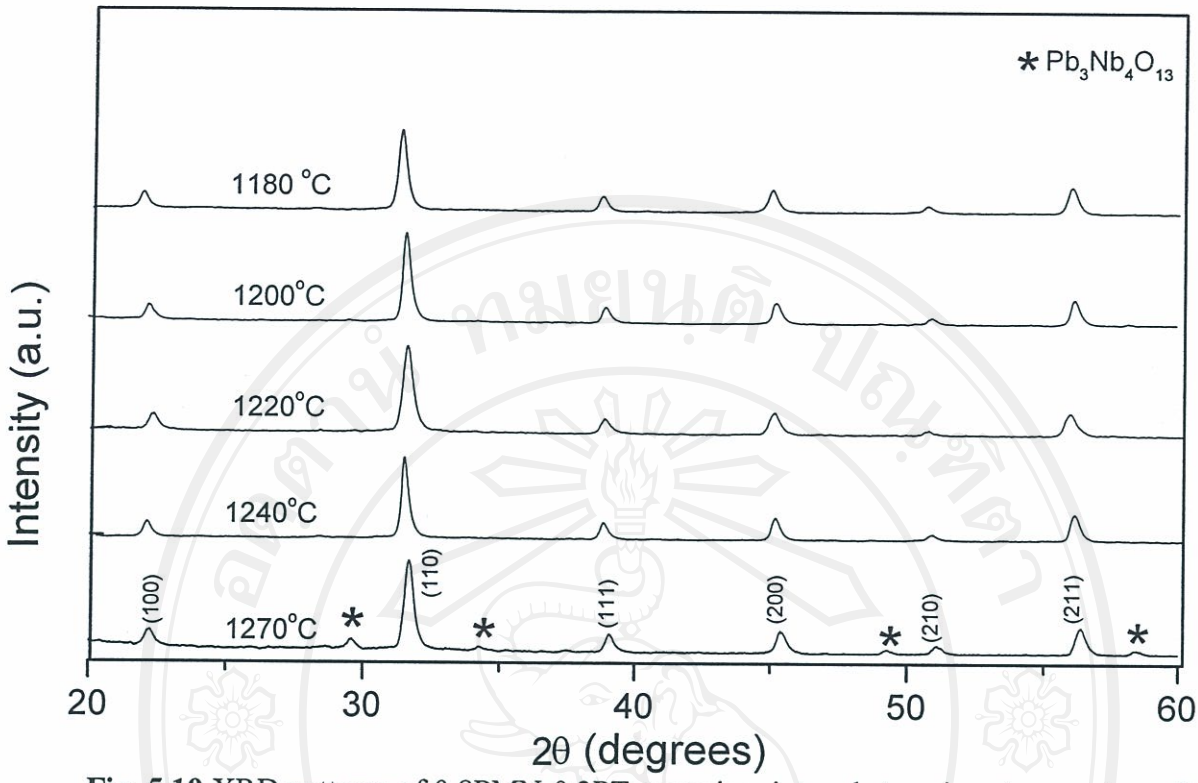

Fig. 5.19 XRD patterns of 0.8PMN-0.2PT ceramics sintered at various temperatures for 2 h with heating/cooling rates at 15 °C/min.

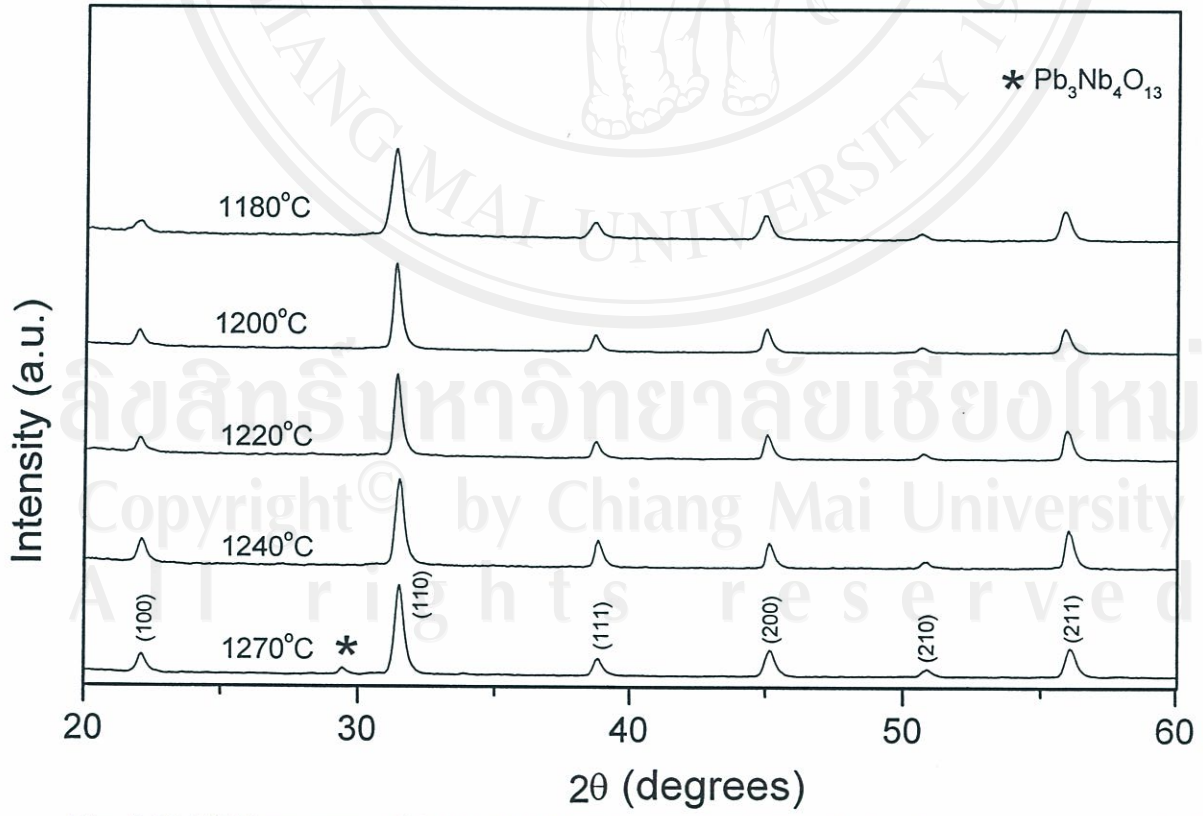

Fig. 5.20 XRD patterns of 0.9PMN-0.1PT ceramics sintered at various temperatures for 2 h with heating/cooling rates at 15 °C/min.

5.3.2 Densification analysis

The densification behavior of all compositions is shown in Fig. 5.21. Density, shrinkage and weight loss data of all compositions after sintered at various conditions are given in Tables 5.4-5.8. As the behavior was similar for all compositions, a density of about 7.40-7.98 g/cm^3 of the maximum value could be achieved in all cases. In general, the bulk density was found to decrease slightly with x, which could be due to the lower melting point of PT compared to PMN. Thus, the admixture of PMN could be considered as a useful technique for promoting the densification of PT, along with its other significant advantage of bringing the Curie range down to lower temperatures as demonstrated by a number of workers.[83-91]

In this study, it is seen that the maximum densification value can be obtained from the samples sintered only at 1240 °C, in samples composition of 0.1 to 0.3 and at 1220 °C, in samples composition of 0.4-0.5. The observed fall-off in density at 1270 °C is probably due both to PbO volatilization impeding the sintering process and the lower density of the pyrochlore phase, which is present with a concentration of ~ 3.52 wt% (see also Table 5.8). This observation is in good agreement with other researchers.[106]

From Figs. 5.22 and 5.23, it can be summerised that shrinkage and weight loss of all compositions increase with sintering temperature in a similar fashion and consistent with those observed in typical lead-based perovskite ceramics.[123]

Table 5.4 Phase formation and densification of 0.5PMN-0.5 PT ceramics sintered at various sintering temperatures.

Sintering temperature (°C)	Perovskite (wt%)	Pyrochlore (wt%)	Density* (g/cm^3)	Shrinkage** (%)	Weight loss*** (%)
1180	100	0.00	7.26	6.02	8.33
1200	100	0.00	7.40	7.54	10.88
1220	100	0.00	7.78	12.40	11.86
1240	100	0.00	7.77	12.97	13.41
1270	100	0.00	7.66	12.94	17.54

* The estimated precision of the density is ± 0.2 %

** The estimated precision of shrinkage is ± 0.3 %

*** The estimated precision of weight loss is ± 0.2%

Table 5.5 Phase formation and densification of 0.6PMN-0.4 PT ceramics sintered at various sintering temperatures.

Sintering temperature (^{o}C)	Perovskite (wt%)	Pyrochlore (wt%)	Density* (g/cm^{3})	Shrinkage* (%)	Weight loss* (%)
1180	100	0.00	7.34	6.84	8.15
1200	100	0.00	7.57	9.27	8.95
1220	100	0.00	7.83	11.10	11.58
1240	98.72	1.28	7.80	12.34	12.39
1270	94.10	5.90	7.64	12.24	18.89

* The estimated precision of the density is ± 0.2 %

** The estimated precision of shrinkage is ± 0.3 %

*** The estimated precision of weight loss is ± 0.2%

Table 5.6 Phase formation and densification of 0.7PMN-0.3 PT ceramics sintered at various sintering temperatures.

Sintering temperature (^{o}C)	Perovskite (wt%)	Pyrochlore (wt%)	Density* (g/cm^{3})	Shrinkage* (%)	Weight loss* (%)
1180	100	0.00	7.38	5.22	7.56
1200	100	0.00	7.63	8.34	9.62
1220	100	0.00	7.72	10.55	10.44
1240	100	0.00	7.86	13.17	12.23
1270	95.67	4.33	7.65	13.24	20.21

* The estimated precision of the density is ± 0.2 %

** The estimated precision of shrinkage is ± 0.3 %

*** The estimated precision of weight loss is ± 0.2%

Table 5.7 Phase formation and densification of 0.8MN-0.2PT ceramics sintered at various sintering temperatures.

Sintering temperature (^{o}C)	Perovskite (wt%)	Pyrochlore (wt%)	Density* (g/cm^{3})	Shrinkage* (%)	Weight loss* (%)
1180	100	0.00	7.39	8.31	6.86
1200	100	0.00	7.63	10.45	8.55
1220	100	0.00	7.77	12.87	10.93
1240	100	0.00	7.94	15.29	12.54
1270	93.67	6.33	7.73	15.54	20.43

* The estimated precision of the density is ± 0.2 %

** The estimated precision of shrinkage is ± 0.3 %

*** The estimated precision of weight loss is ± 0.2%

Table 5.8 Phase formation and densification of 0.9MN-0.1PT ceramics sintered at various conditions.

Sintering temperature (°C)	Dwell times (h)	Heating/cooling rates (°C/min)	Perovskite (wt%)	Pyrochlore (wt%)	Density* (g/cm^3)	Shrinkage** (%)	Weight loss*** (%)
1180	2	15	100.00	0.00	7.40	9.01	7.34
1200	2	15	100.00	0.00	7.64	11.86	9.11
1220	2	15	100.00	0.00	7.80	13.24	11.01
1240	1	15	100.00	0.00	7.79	12.96	10.98
1240	2	15	100.00	0.00	7.98	14.92	12.84
1240	4	15	97.96	2.04	7.86	14.97	14.77
1240	6	15	95.11	4.89	7.67	14.99	16.82
1240	2	3	95.78	4.22	7.71	14.91	15.32
1240	2	5	97.44	2.56	7.89	14.92	13.98
1240	2	10	100.00	0.00	7.97	14.93	12.86
1240	2	30	100.00	0.00	7.92	14.90	12.81
1270	2	15	96.48	3.52	7.75	14.97	15.21

* The estimated precision of the density is ± 0.2 %

** The estimated precision of shrinkage is ± 0.3 %

*** The estimated precision of weight loss is ± 0.2%

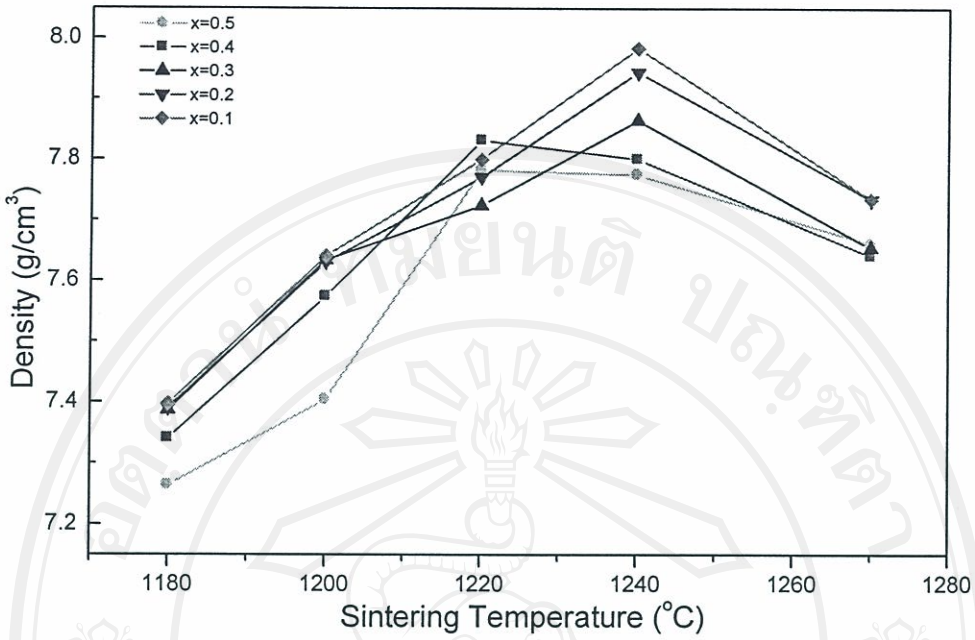

Fig. 5.21 Dependence of bulk density on sintering temperature for (1-*x*)PMN-*x*PT ceramics.

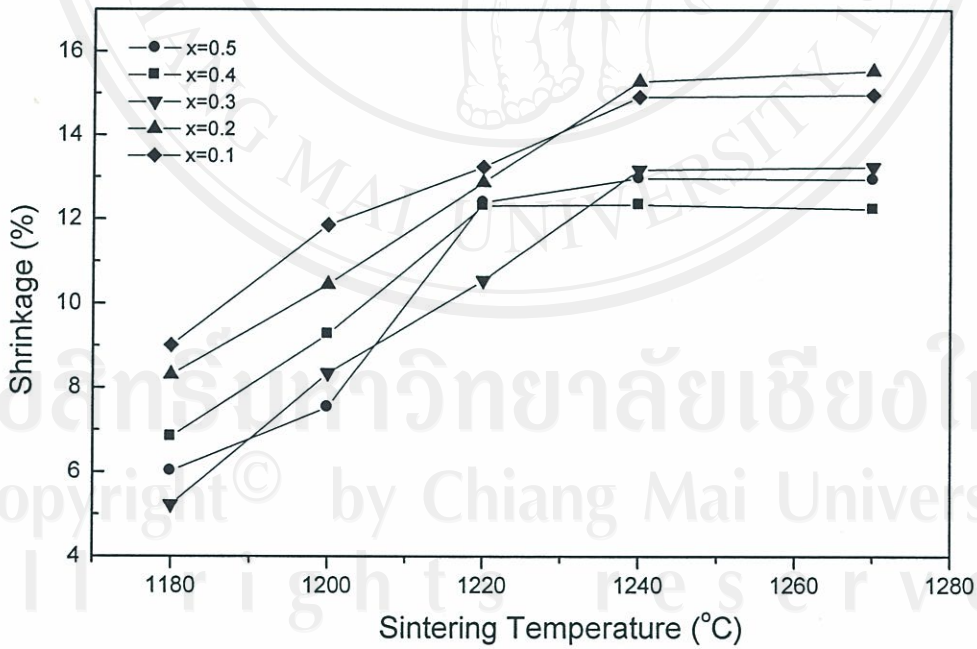

Fig. 5.22 Dependence of shrinkage on sintering temperature for (1-*x*)PMN-*x*PT ceramics.

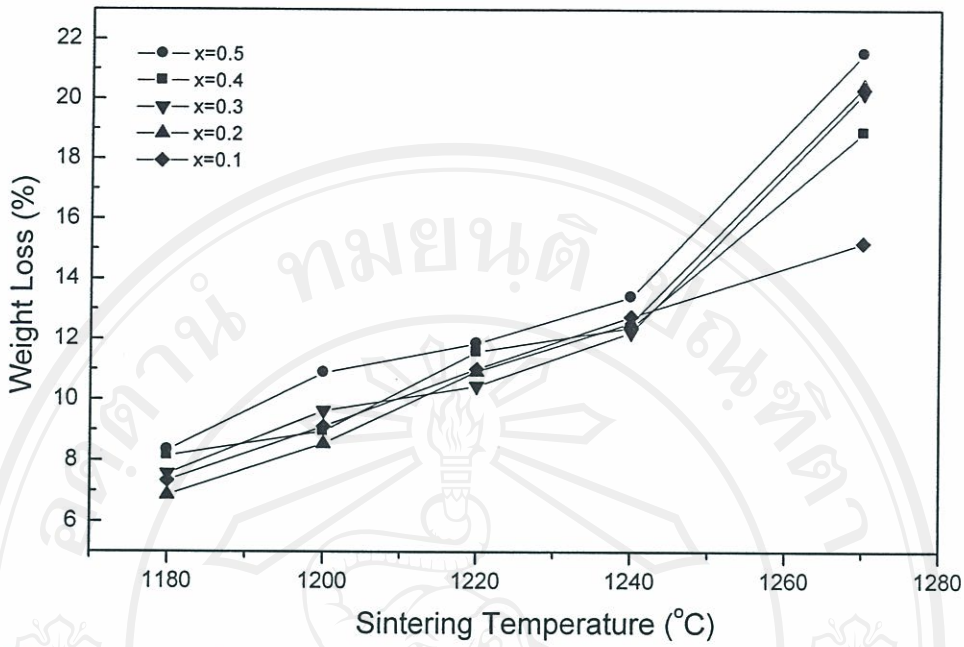

Fig. 5.23 Dependence of weight loss on sintering temperature for 0.9PMN-0.1PT ceramics.

5.3.3 Microstructral analysis

SEM-micrographs of both as fired and fracture surfaces of all compositions are shown in Fig. 5.24, indicating representative microstructures. These samples were sinterd at their optimum temperatures. In general, similar microstructral characteristics were observed in these samples, i.e. uniformly sized grains with a high degree of grain close-packing. Almost no abnormal grain growth was observed, although some small particles with diameter about 0.28-0.55 μm were found at the grain boundaries and triple junctions of some samples (e.g. 0.8PMN-0.2PT). By applying the linear intercept method to these SEM micrographs, mean grain sizes of about 0.3-3.35 μm were estimated for these samples as given in Table 5.9. It should be seen as a rough approximation since the micrographs exhibit only 2 dimensional images of the unpolished samples.

Apart from the grain size, the effect of chemical composition on the grain shape was also found to be quite significant (Fig. 5.25). In the present study, an attempt was made to determine the grain shape by employing the concept of the degree of angularity under the ASTM D 2488-90 regulation[114] (Table 5.9). In this connection, it is shown that the degree of angularity is found to increase gradually with PT content (x) for the compositions with $0.1 \leq x \leq 0.5$.

In this work, (1-x)PMN-xPT ceramics with a high degree of grain close-packing microstructures can be effectively achieved by sintering an appropriate PMN-PT powders, employing straightforward techniques. However, small amounts of MgO, PbO and pyrochlore phase can still be detected, indicating their poor reactiveties due to the limitation of a mixed oxide processing.

Table 5.9 Grain sizes and degree of angularity of (1-x)PMN-xPT ceramics sintered at their optimum temperature.

Composition (x)	Grain size* (μm)	Degree of angularity
0.1	0.42-3.66	100-199
0.2	0.44-3.02	200-299
0.3	0.41-2.80	300-399
0.4	0.41-3.45	300-499
0.5	0.48-3.72	500-699

* These data were taken by estimating from SEM-micrographs

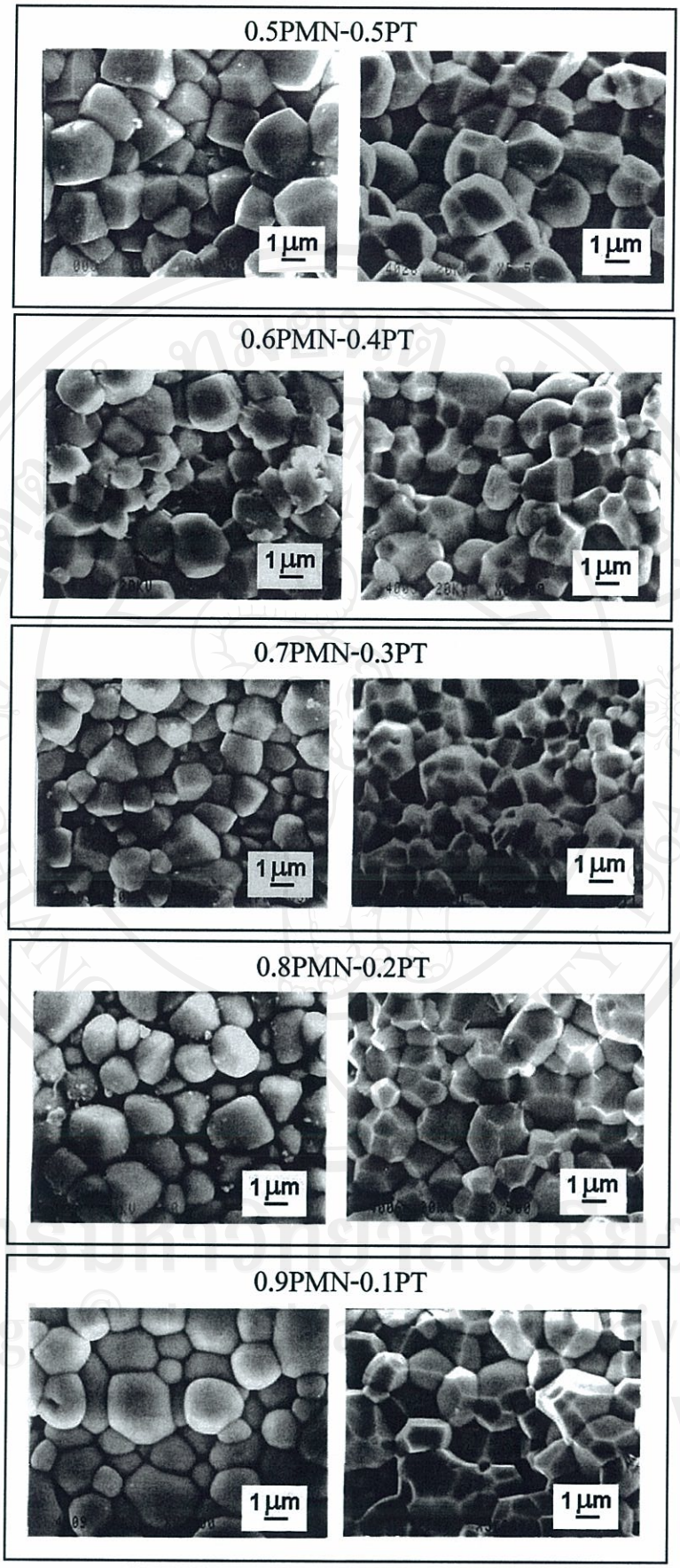

Fig. 5.24 SEM micrographs of free surfaces and fractures of PMN-PT various compositions sintered at their optimum temperature.

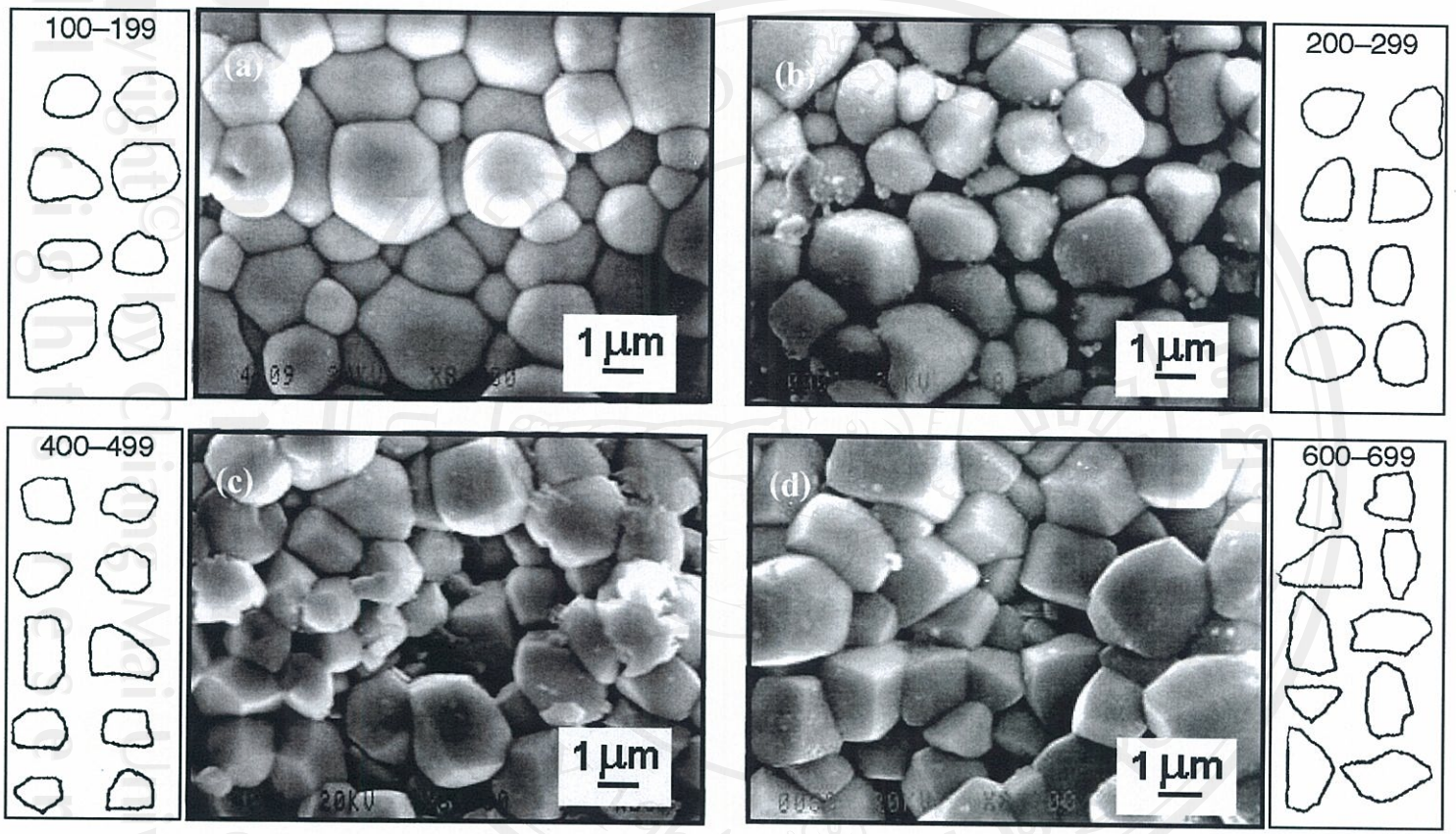

Fig. 5.25 Degree of angularity of (1-x) PMN-xPT ceramics sintered at their optimum temperature, (a) $x = 0.1$ (b) $x = 0.2$ (c) $x = 0.4$, and $x = 0.5$.

5.4 Ceramics in the 0.9PMN- 0.1PT system

Although a number of inter-relationships between the chemical compositions and phase formation behavior of PMN-PT ceramics have been observed in the previous section, one must be careful not to underestimate the importance of sintering conditions. In this connection, the effect of sintering schedule on phase formation behavior of each composition was also examined.

5.4.1 Phase analysis

X-ray diffraction patterns of 0.9PMN-0.1PT ceramics sintered at various conditions are given in Figs. 5.26-5.28, indicating the formation of both perovskite and pyrochlore phases in each case. The strongest reflections in the majority of the XRD patterns indicate the formation of perovskite phase of lead magnesium niobate-lead titanate, 0.9PMN-0.1PT. In this study, a single phase of perovskite 0.9PMN-0.1PT was found in the samples sintered at temperature between 1180 and 1240 °C. After sintering at 1270 °C, small amounts of second phase could be detected by XRD, with additional reflections (marked by *), correlating with a pyrochlore phase of composition $Pb_3Nb_4O_{13}$ (JCPDS file no. 25-443) commonly found in the fabrication of PMN-based materials.[20] This could be due to the higher firing temperature leading to volatility of lead oxide and increased tendency to form pyrochlore, in good agreement with other works.[123,136]

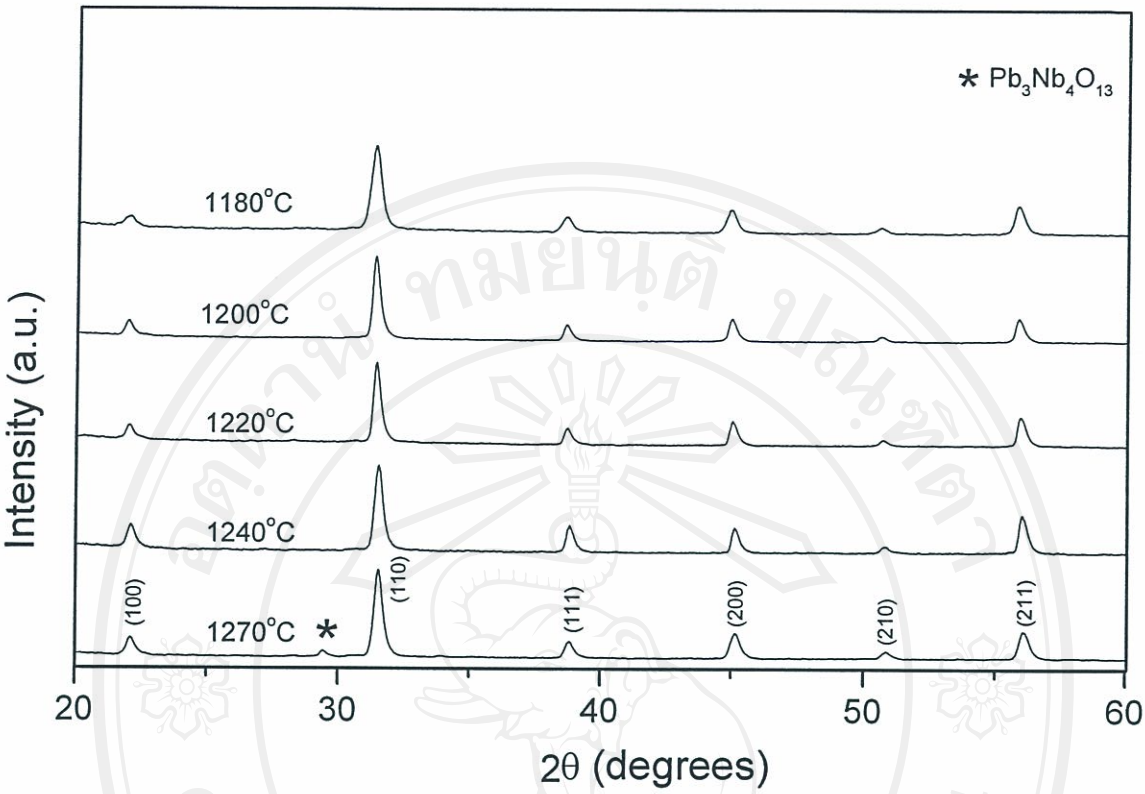

Fig. 5.26 XRD patterns of 0.9PMN-0.1PT ceramics sintered at various temperatures for 2 h with heating/cooling rates at 15 °C/min.

Having established the optimum sintering temperature, alternative dwell times of 1, 2, 4, and 6 h with constant heating/cooling rates of 15 °C/min were applied at 1240 °C, as shown in Fig. 5.27. The single phase of perovskite 0.9PMN-0.1PT was found to be possible only in ceramics, sintered at 1240 °C with dwell time of 2 h or less. The appearance of $Pb_3Nb_4O_{13}$ phase could be attributed to the loss of PbO after prolonged dwell time, which causes the decomposition of perovskite to pyrochlore. Similar result was also reported by other workers.[137]

Apart from the sintering temperature and dwell time, the effect of heating/cooling rates on phase formation behavior of 0.9PMN-0.1PT ceramics was also examined. Five heating/cooling rates (3, 5, 10, 15 and 30 °C/min) were selected for sintering condition of 1240 °C/ 2 h (Fig. 5.28). In this connection, it is shown that

only fast heating/cooling rates can lead to full crystallization of 0.9PMN-0.1PT phase without time for the lead vaporization or the formation of pyrochlore phase, in agreement with Liou *et al.*[123] The observation that faster heating/cooling rates are required for lead-based ferroelectrics is also consistent with other investigators.[116]

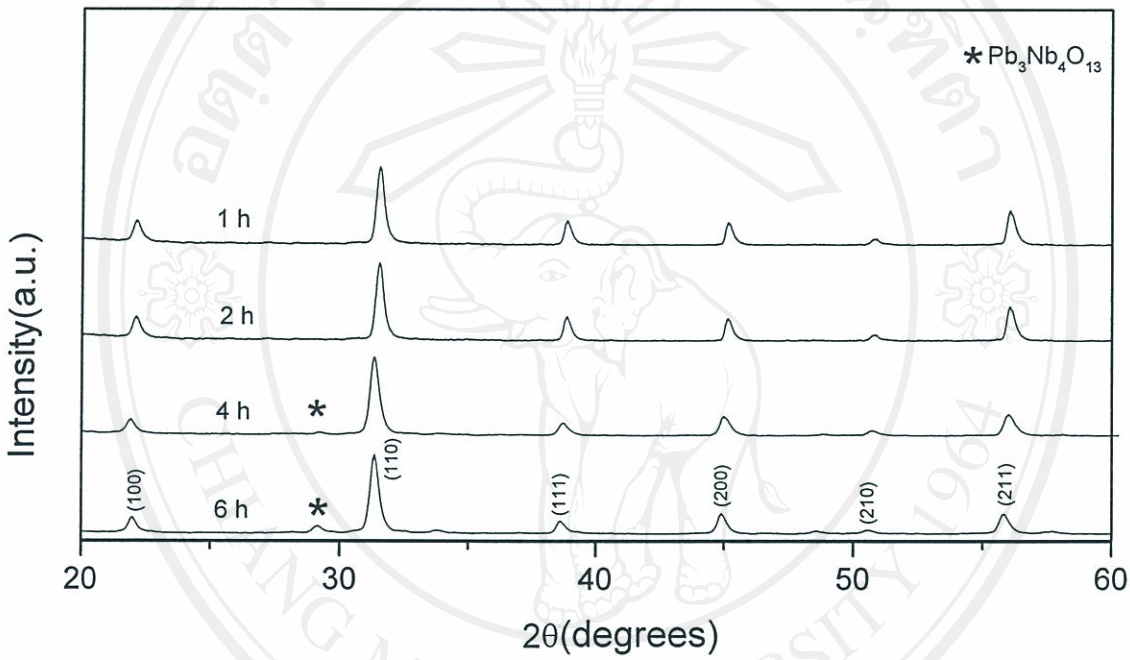

Fig. 5.27 XRD patterns of 0.9PMN-0.1PT ceramics sintered at 1240 °C with heating/cooling rates of 15 °C/min for various dwell times.

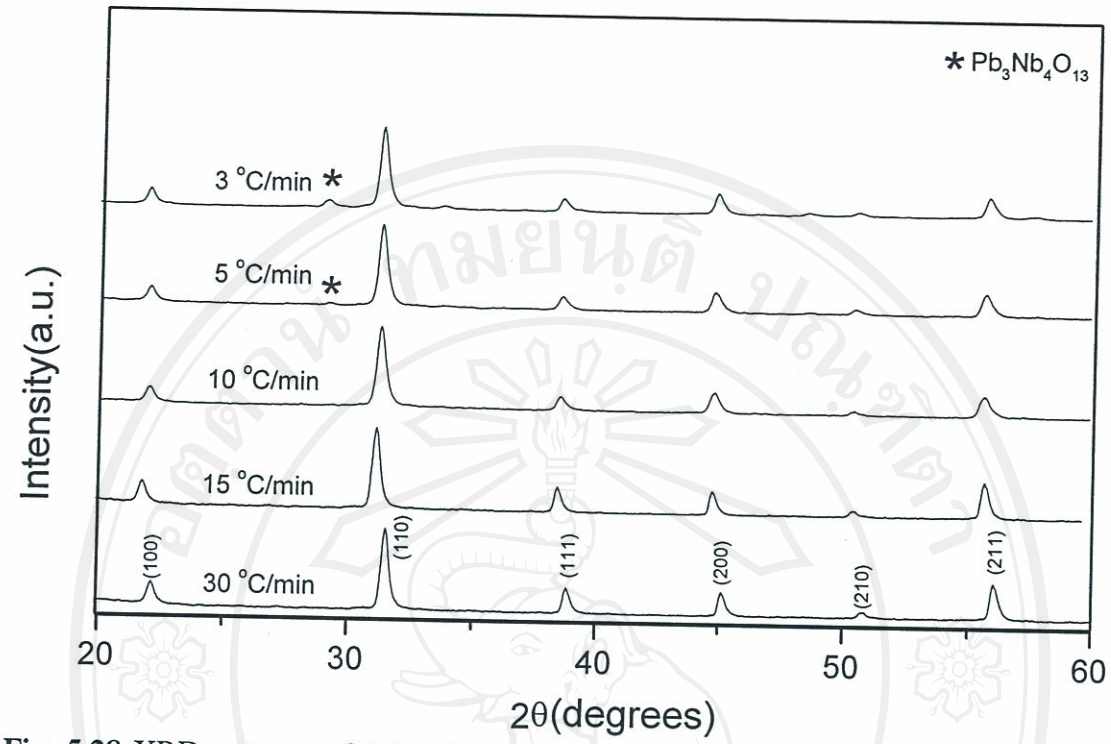

Fig. 5.28 XRD patterns of 0.9PMN-0.1PT ceramics sintered at 1240 °C for 2 h with various heating/cooling rates.

5.4.2 Densification analysis

Density, shrinkage and weight loss data of 0.9PMN-0.1PT ceramics sintered at various conditions are summarized in Table 5.8. It is observed that a density of about 7.40-7.98 g/cm^3 of the maximum value for 0.9PMN-0.1PT can be achieved in this study. The maximum density was obtained in the samples sintered at 1240°C for 2 h with heating/cooling rate of 15 °C/min. By comparing with those of 0.9PMN-0.1PT ceramics produced by reaction-sintering process[137], densities of 8.07 and 8.03 g/cm^3 were comparable for samples sintered at 1230 °C for 2 and 4 h, respectively. From Fig. 5.29, the observed fall-off in density at higher temperature is probably due both to evaporate of PbO impeding the sintering process and lower density of pyrochlore phase, which is present with concentration of ~ 3.52 wt% (see also Table 5.8). These results supported by some related work of James *et al.*[140],

which demonstrated that lead loss due to either inappropriate heating rate or high sintering temperature invariably leads to PbO-deficient pyrochlore ($Pb_3Nb_4O_{13}$) being formed. Moreover, they have found that PbO deficiency can result in not only excessive presence of pyrochlore phase, but also poor density of the samples.

The effect of dwell times on the densification of 0.9PMN-0.1PT ceramics sintered at 1240 °C with heating/cooling rate of 15 °C/min are shown in Fig. 5.30. It is seen that density increases as dwell time increases from 1 to 2 h and decreases at higher dwell time. Apart from the sintering temperature and dwell time, the effect of heating/cooling rates on the densification behavior of 0.9PMN-0.1PT ceramics was also investigated. It is found that density increases as the rate increases from 3 to 5 °C/min and stables at higher rates (Fig. 5.31).

Shrinkage and weight loss data of 0.9PMN-0.1PT ceramics sintered at various conditions are shown in Figs. 5.32-5.34. The change in dimension was gradually increased with sintering temperature at 1180 °C to 1240 °C and approximately constant after 1240 °C. As would be expected, the linear shrinkage is found to increase with the sintering temperature and dwell time. Whereas, in term of the effect of heating/cooling rates, a gradual increase in the linear is observed with increasing the rates from 3 to 5 °C/min and then decrease at higher rates.

It is interesting to note that a weight loss of 0.9PMN-0.1PT ceramics during sintering increases with sintering temperature and dwell times but did not vary significantly with heating/cooling rates, in consistent with the densification results.

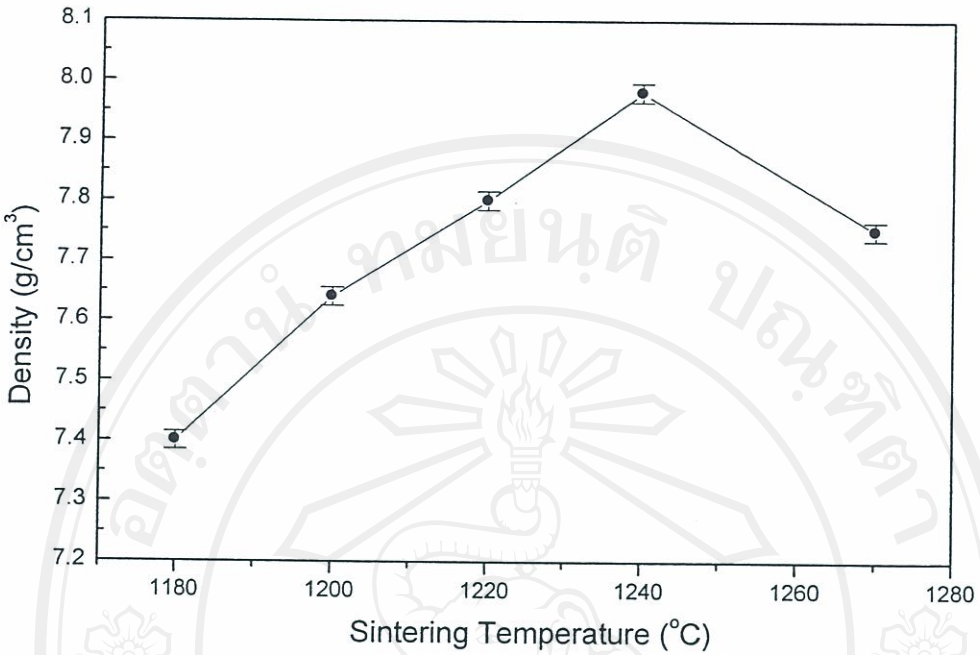

Fig. 5.29 Dependence of bulk density on sintering temperature for 0.9PMN- 0.1PT ceramics.

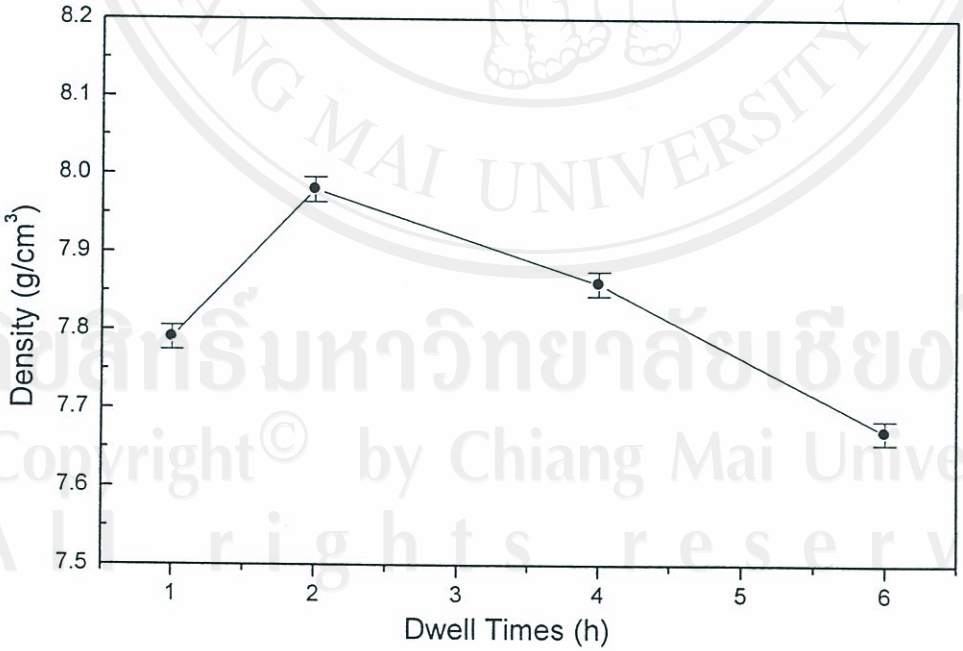

Fig. 5.30 Dependence of bulk density on dwell time for 0.9PMN-0.1PT ceramics at 1240 °C.

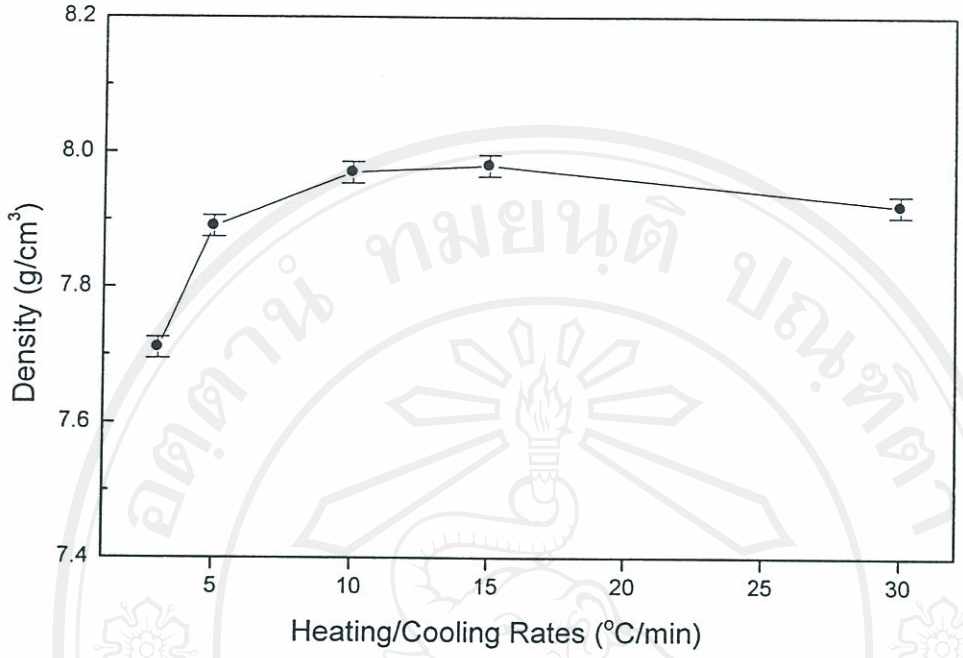

Fig. 5.31 Dependence of bulk density on heating/cooling rates for 0.9PMN-0.1PT ceramics at 1240 °C for 2 h.

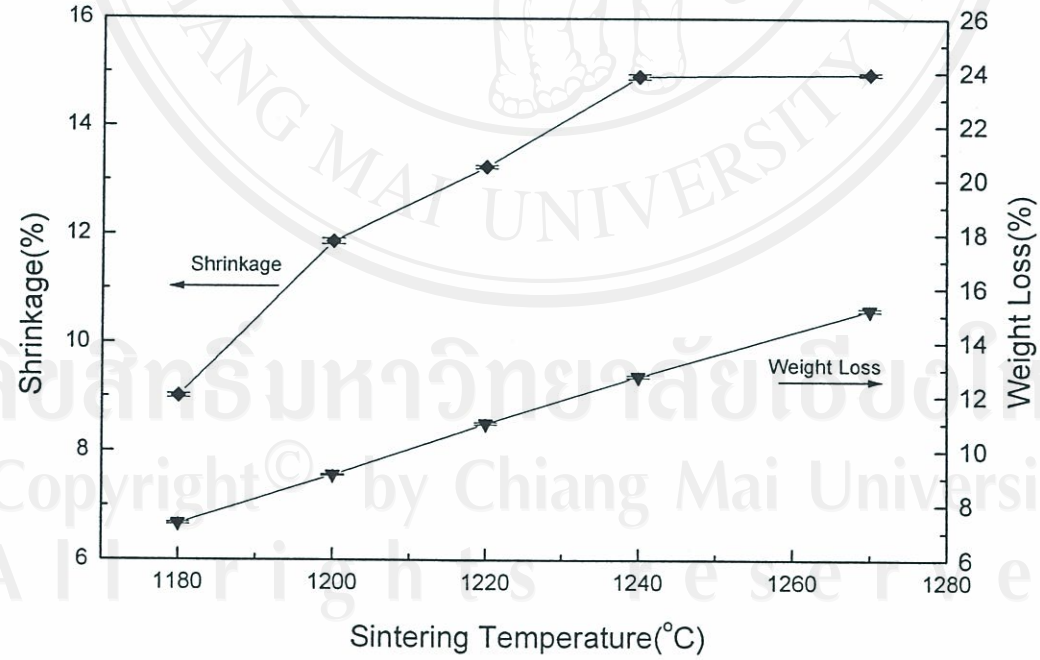

Fig. 5.32 Dependence of shrinkage and weight loss on sintering temperature for 0.9PMN-0.1PT ceramics.

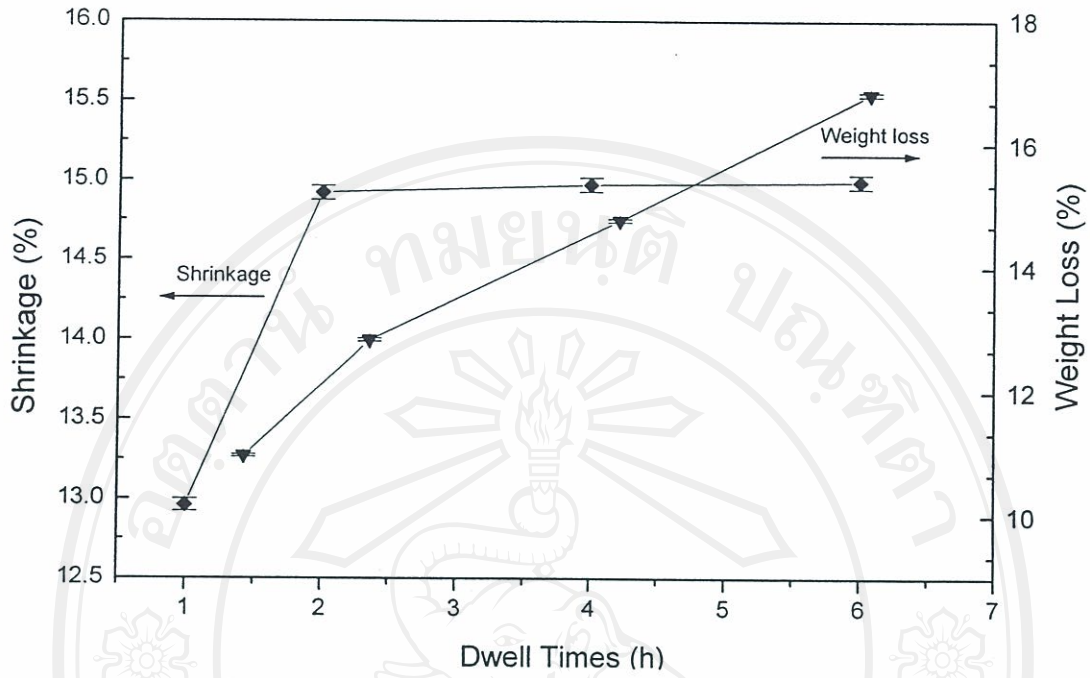

Fig. 5.33 Dependence of shrinkage and weight loss on dwell times for 0.9PMN-0.1PT ceramics at 1240 °C.

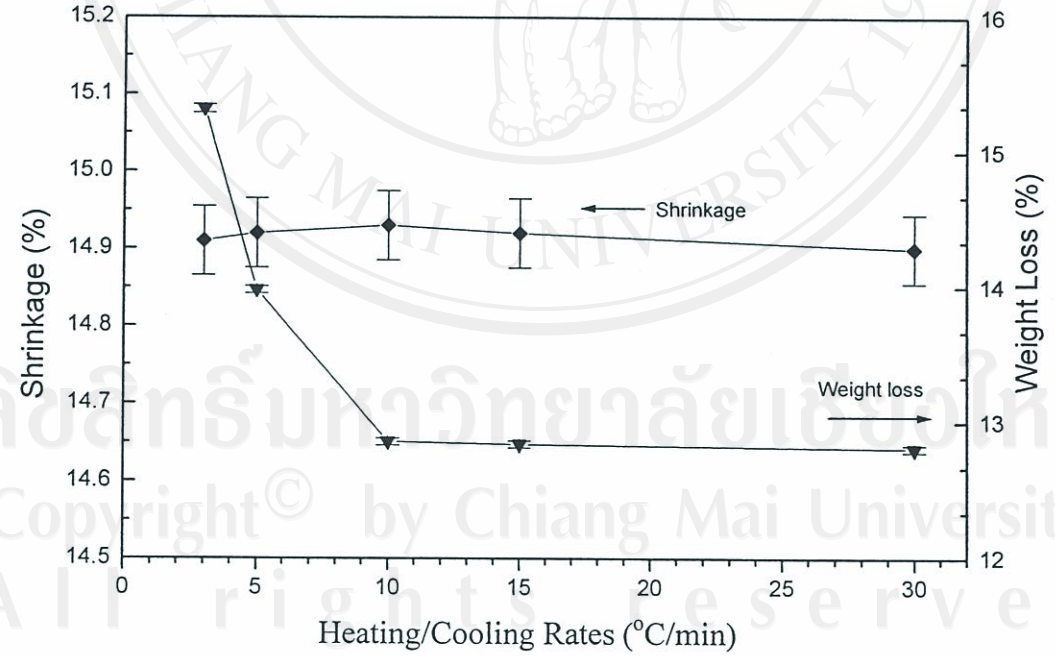

Fig. 5.34 Dependence of shrinkage and weight loss on heating/cooling rates for 0.9PMN-0.1PT ceramics sintered at 1240 °C for 2 h.

5.4.3 Microstructural analysis

Further microstructural analysis was performed on the selected samples of 0.9PMN-0.1PT by a combination of scanning electron microscopy (SEM) and energy dispersive X-ray analysis (EDX) of free and fracture surface micrographs 0.9PMN-0.1PT ceramics sintered at various temperatures from 1200 to 1240 °C are shown in Fig. 5.35. The results indicate that grain size tend to increase with sintering temperature, in agreement with other work.[107,134,137] The microstructure becomes denser as the sintering temperature increase up to 1240 °C, as indicated by the grain packing and increases in grain boundary thickness.

Figure 5.36 shows SEM micrographs of 0.9PMN-0.1PT ceramics sintered at 1240 °C with different dwell times. It is seen that the grain size varies significantly as a function of dwell times. The appearance of pyrochlore phase can be attributed to volatilization of PbO from perovskite matrix. Similar results was also observed by Kong *et al.*[134] However, average grain sizes of 0.9PMN-0.1PT ceramics did not vary significantly with heating/cooling rates as shown in Fig. 5.37. It should be that noted at higher dwell times and lower heating/cooling rates, some phases (white) appear which appear in the form of elongated platelets and/or as long needles were identified as PbO-rich compositions. The characteristic morphology of platelets and needles suggests that these phases have probably formed during cooling by crystallizing from the melt, in consistent with Guha.[122]

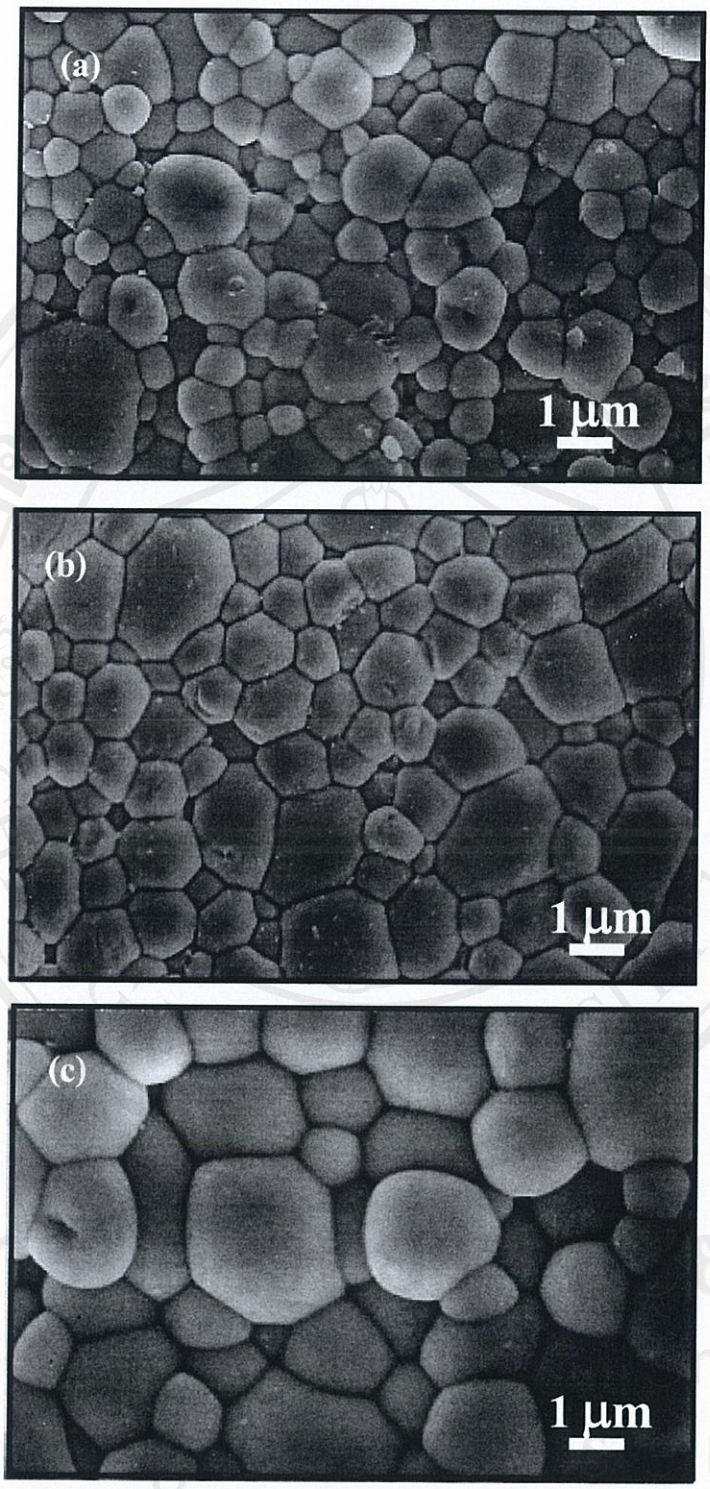

Fig. 5.35 SEM micrographs of free surfaces of 0.9PMN-0.1PT ceramics sintered at (a) 1200 °C, (b) 1220 °C and (c) 1240 °C, for 2 h with heating/cooling rates of 15 °C/min.

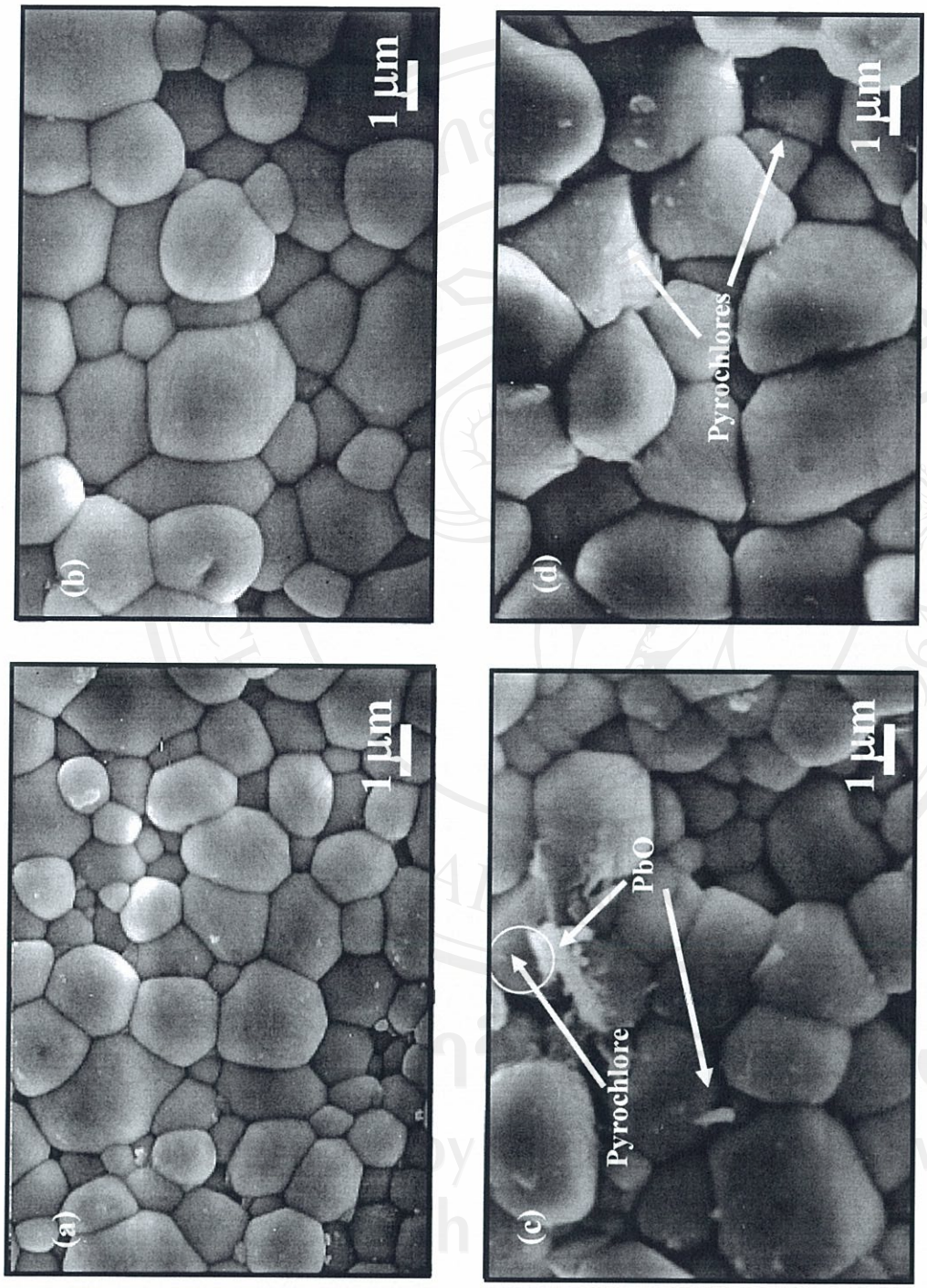

Fig. 5.36 SEM micrographs of free surfaces of PMN ceramics sintered at 1240 °C with heating/cooling rates of 15 °C/min for (a) 1, (b) 2, (c) 4 and (d) 6 h.

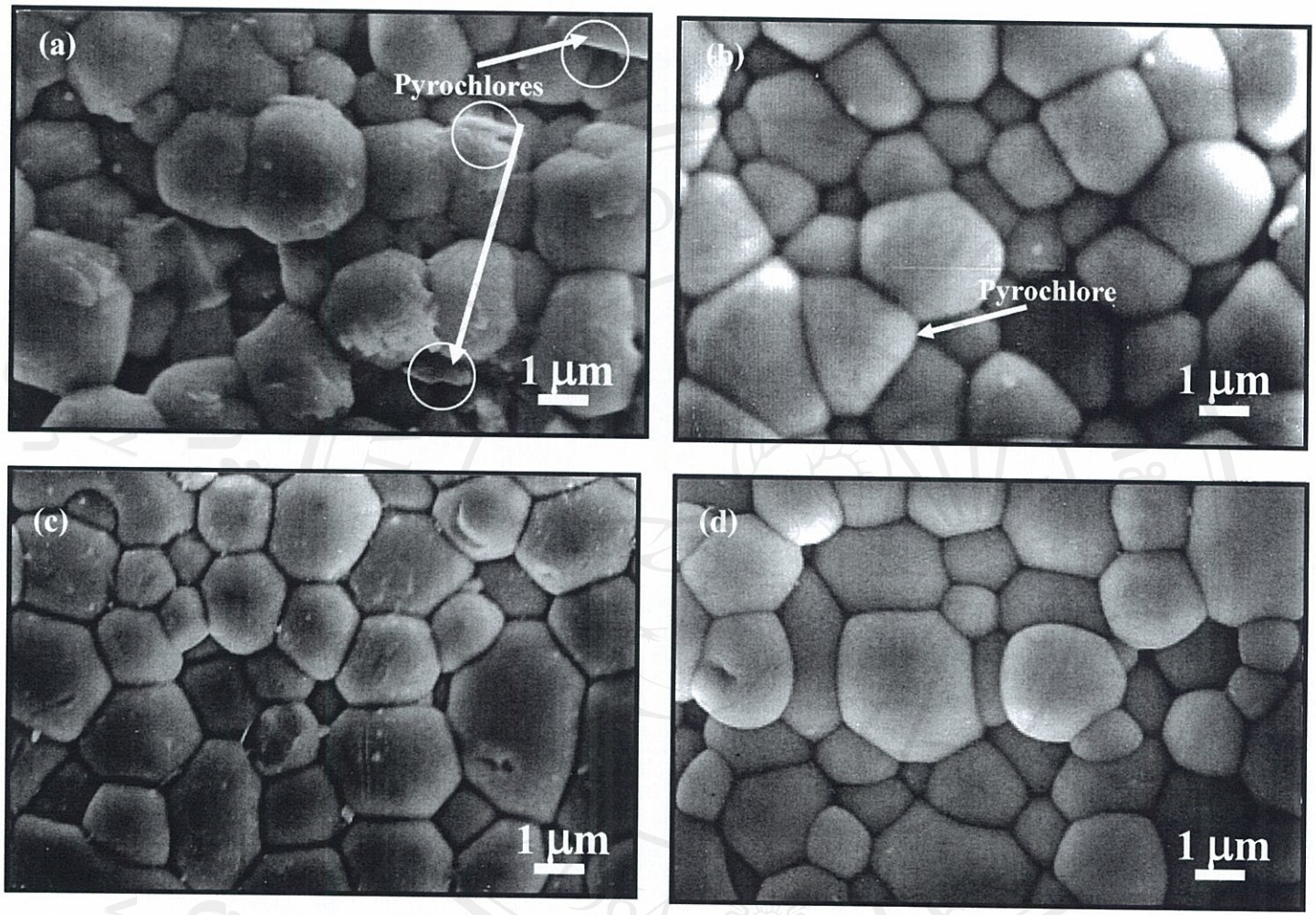

Fig. 5.37 SEM micrographs of free surfaces of 0.9PMN-0.1PT ceramics sintered at 1240 °C for 2 h with heating/cooling rates of (a) 3, (b) 5, (c) 10 and (d) 15 °C/min.